Title

ERF and WRKY transcription factors regulate *IDA* and abscission timing in Arabidopsis.

Author information

Sergio Galindo-Trigo[1]*(s.g.trigo@ibv.uio.no), Anne-Maarit Bågman[2](ambagman@ucdavis.edu), Takashi Ishida[3,4](ishida-takashi@kumamoto-u.ac.jp), Shinichiro Sawa[4](sawa@kumamoto-u.ac.jp), Siobhán M. Brady[2](sbrady@ucdavis.edu), Melinka A. Butenko[1]*(m.a.butenko@ibv.uio.no).

[1] Section for Genetics and Evolutionary Biology, Department of Biosciences, University of Oslo, Norway.

[2] Department of Plant Biology and Genome Center, University of California, Davis, USA.

[3] International Research Organization for Advanced Science and Technology (IROAST), Kumamoto University, Kumamoto, Japan.

[4] Graduate School of Science and Technology, Kumamoto University, Kumamoto, Japan.

* For correspondence: s.g.trigo@ibv.uio.no, m.a.butenko@ibv.uio.no

Submission date

13th of September 2023.

Items in the manuscript

Five main figures; Twelve supplemental figures; Three supplemental tables.

Word count

5199 words (excluding Materials and methods).

Running title

ERFs and WRKYs transcriptionally regulate *IDA*.

Highlight

ERF and WRKY transcription factors distinctly contribute to the regulation of *IDA* expression and thereby abscission timing. WRKY57 modulates abscission via redundant IDA/IDA-like peptides.

Abstract

Plants shed organs like leaves, petals or fruits through the process of abscission. Monitoring cues like age, resource availability, biotic and abiotic stresses allows plants to abscise organs in a timely manner. How these signals are integrated in the molecular pathways that drive abscission is largely unknown. The *INFLORESCENCE DEFICIENT IN ABSCISSION* (*IDA*) gene is one of the main drivers of floral organ abscission in Arabidopsis and is known to transcriptionally respond to most abscission-regulating cues. Interrogating the *IDA* promoter *in silico* and *in vitro* we identified transcription factors that can potentially modulate *IDA* expression. We functionally characterized the importance of ERF and WRKY binding sites for *IDA* expression during floral organ abscission, with WRKYs being of special relevance to mediate *IDA* upregulation in response to biotic stress in tissues destined for separation. We further characterized WRKY57 as a positive regulator of *IDA* and *IDA-like* gene expression in abscission zones. Our findings highlight the promise of promoter element-targeted approaches to modulate the responsiveness of the IDA signaling pathway to harness controlled abscission timing for improved crop productivity.

Keywords

Abscission, cis-elements, ERF, IDA, promoter, signaling, transcription, WRKY.

Abbreviations

Abscission zone (AZ), Ethylene response factor (ERF), HAESA (HAE), INFLORESCENCE DEFICIENT IN ABSCISSION (IDA), IDA-like (IDL), Microbe-Associated Molecular Pattern (MAMP), Transcription factor (TF), TF binding sites (TFBS), Yeast one-hybrid (Y1H).

Introduction

Abscission is the developmentally programmed process of cell separation. Indeterminate growth and a modular developmental plan allow plants to shed organs that are no longer needed. Abscission can take place in leaf petioles, floral organs, flower pedicels, fruits or seeds, to name a few. The ubiquitous presence of abscission across plant organs and developmental phases provides these sessile organisms with flexibility to prioritize resource allocation and a very effective strategy to minimize disease spread. On the other hand, untimely or uncontrolled abscission has profound negative consequences for agriculture. Indeed, as humankind has domesticated plants, seed abscission has been selected against in crops, hindering a process that naturally evolved to aid seed dispersal in benefit of more efficient and plentiful harvests (Pickersgill, 2007). Controlled abscission is still actively sought-after in breeding programs. Understanding the complex set of cues that influence abscission occurrence or its timing is thus highly relevant.

There is a broad spectrum of cues that influence abscission. The phytohormones auxin and ethylene have antagonistic effects on abscission (Addicott et al., 1955; Abeles and Rubinstein, 1964; Louie Jr and Addicott, 1970; Elmo M. Beyer and Morgan, 1971; Meir et al., 2006; Meir et al., 2010; Basu et al., 2013; Meir et al., 2015). The generally accepted model suggests the competence to abscise is blocked by auxin efflux from the organ into the abscission zone (AZ). Ethylene is a positive effector of abscission and ethylene sensitivity acquisition is a milestone for abscission induction (Abeles and Rubinstein, 1964; Burg, 1968; Reid, 1985; Brown, 1997; Cin et al., 2005; Merelo et al., 2017; Botton and Ruperti, 2019). Carbohydrate availability is a well-known factor regulating abscission induction (Sawicki et al., 2015). Carbohydrate starvation triggers abscission, as documented in multiple plant species after shading or defoliation (Addicott et al., 1955; Aloni et al., 1997; Peng et al., 2013). Exogenous cues like water availability and pathogens also regulate abscission induction (Patharkar and Walker, 2016; Reichardt et al., 2020). Plants sense infections in leaves and trigger abscission to diminish the spread of the disease (Ketring and Melouk, 1982; Ben-David et al., 1986; Glick et al., 2009; Scalschi et al., 2014). Other phytohormones (cytokinin, salicylic acid, jasmonic acid), developmental cues (senescence, fruit and seed development), as well as exogenous cues (light and temperature) are known to influence abscission (for review, see (Ma et al., 2021)). Understanding how the molecular pathways that execute abscission integrate these complex signals would greatly inform abscission-related breeding programs.

The abscission of floral organs in *Arabidopsis thaliana* (Arabidopsis) is the best characterized abscission model. AZs develop at the base of each floral organ (sepals, petals, and stamens) as two adjacent but distinct cell layers: the residuum and secession layers. Secession cells are located proximal to the abscising organ and form a lignified structure called lignin brace. The lignin brace is thought to focus cell wall degrading enzyme activity and provide local rigidity to facilitate shedding (Lee et al., 2018). Residuum cells make up the cell layer that remains on the flower receptacle after abscission occurs, differentiating into cuticle-bearing epidermal-like cells. Several transcription factors (TFs) are necessary for AZs to differentiate during flower development, including BLADE ON PETIOLE 1 (BOP1) and BOP2, ARABIDOPSIS THALIANA HOMEOBOX GENE 1 (ATH1), KNOTTED-LIKE FROM ARABIDOPSIS THALIANA 2 (KNAT2) and KNAT6 (McKim et al., 2008; Crick et al., 2022). When abscission zones have developed and floral organs are no longer required, abscission zones secrete the peptide INFLORESCENCE DEFICIENT IN ABSCISSION (IDA) to trigger the cell separation (Butenko et al., 2003). IDA is perceived in the AZ cells by leucine-rich repeat (LRR) receptor kinases (RKs) HAESA (HAE) and HAESA-LIKE 2 (HSL2) and their co-receptors, members of the family of somatic embryogenesis receptor kinases (SERKs; (Jinn et al., 2000; Cho et al., 2008; Stenvik et al., 2008; Meng et al., 2016; Santiago et al., 2016)). When the HAE-SERK/HSL2-SERK receptor complexes activate, they trigger an intracellular signaling cascade of MITOGEN-ACTIVATED PROTEIN KINASES (MAPKs; (Cho et al., 2008; Zhu et al., 2019)). The MAPK cascade inhibits negative transcriptional regulators of abscission, KNAT1 and AGAMOUS-LIKE 15, thereby allowing the progression of abscission (Wang et al., 2006; Shi et al., 2011; Butenko et al., 2012; Patharkar and

Walker, 2015). Other regulators influence abscission indirectly by modulating the IDA-induced signaling pathway (Liljegren et al., 2009; Leslie et al., 2010; Burr et al., 2011; Liu et al., 2013; Gubert and Liljegren, 2014; Baer et al., 2016; Taylor et al., 2019)

The signaling cascade induced by IDA and HAE/HSL2 in AZs is a requisite for floral organ abscission. Double mutants *hae hsl2* retain all floral organs across floral positions in the inflorescence (Cho et al., 2008; Stenvik et al., 2008). Meanwhile, *ida* knockouts display a weaker abscission phenotype, with floral organs being loosely attached in floral positions in which siliques are elongating (Stenvik et al., 2008; Alling and Galindo-Trigo, 2023). The weaker abscission phenotype in *ida* mutants is likely due to functional redundancy with related IDA-like (IDL) peptides in AZs (Stenvik et al., 2008; Vie et al., 2015). A recent revisitation of the literature has proposed the IDA pathway could be responsible for the very last steps of separation mediating an increase in turgidity and cell expansion, while abscission activation and initiation of cell wall degradation would be mostly dependent on ethylene signaling (Meir et al., 2019). In this scenario, IDA would be one of several responses that ethylene activates in AZs to orchestrate the separation of floral organs. AZ promoter activity of *IDA* was indeed found to depend on ethylene signaling (Butenko et al., 2006). Wounding was also shown to induce early activation of *IDA* promoter in AZs (Butenko et al., 2006). In cauline AZs, drought stress induces *IDA* transcription (Patharkar and Walker, 2016). In the lateral root emergence zone of seedlings, *IDA* promoter activity is enhanced in response to the Microbe-Associated Molecular Patterns (MAMPs) flagellin (flg22), chitin, as well as to salt and mannitol (Lalun et al., 2023). These instances suggest that a sizeable set of environmental factors known to influence abscission are integrated in the transcriptional regulation of *IDA*.

In this study, we investigate the genetic and molecular determinants of *IDA* transcriptional regulation. An *in silico* dissection of the *IDA* promoter and a screen against an Arabidopsis TF collection highlight the diversity of cues and effectors that can modulate *IDA* expression. We demonstrate that DNA binding sites of ethylene response factors (ERFs) and WRKY TFs are required for full transcriptional competence of *IDA* and to mediate its MAMP-dependent transcriptional upregulation, respectively. We also show that WRKY57 can modulate floral organ abscission in an IDA/IDL and HAE/HSL2-dependent manner.

Materials and methods

Plant material, growth conditions and treatments

All Arabidopsis lines were in the Columbia (Col-0) genetic background, except for the *ida-1* mutant (C24; (Butenko et al., 2003)). The previously published mutant and transgenic lines used in this study were: *ida-2* (Cho et al., 2008), *idaCR* (Alling and Galindo-Trigo, 2023), *idl1CR* (Shi et al., 2018), *p35S::IDA* (Stenvik et al., 2006), *hae hsl2* (Stenvik et al., 2008), *wrky57* (Jiang et al., 2012), *wrky60-1* (Xu et al., 2006) and *wrky48* (Jiang et al., 2012). Genotyping primers are listed in the Supplemental Table S1.

Arabidopsis plants were routinely vapor-sterilized with chlorine gas, sown on Murashige & Skoog (MS) medium plates with 0.7% sucrose, stratified for three days and germinated in growth chambers for a week before transfer to regular sowing soil. Subsequently, plants grew in climate rooms until seed setting and senescence. Environmental growth conditions in the growth chamber and climate rooms were similar: photoperiod of 16h day/8h night, light intensity of 130-150 $\mu mol \cdot m^{-2} \cdot s^{-1}$, temperature of 22ºC, and 60% humidity. Transgenic plants were selected in plates supplemented with Basta or hygromycin-B as required. Microscopy of roots was carried out with vertically grown seedlings in 0.5xMS plates with 0.7% sucrose.

In the case of the flg22-treated mature rosette leaves, seeds were directly germinated on peat pellets (Jiffy 7) with short day photoperiod (10h day/14h night). Two plants per pellet were allowed to progress past seedling stage. At week 6 and prior to bolting, the most expanded rosette leaf of each plant was

97 syringe infiltrated with mock solution (water) or flg22 solution (500 nM flg22 in water). Twenty hours
98 later, leaves were detached and individually processed to detect GUS activity. Leaves were assigned to
99 different qualitative categories with values ranging from 0 (undetectable GUS staining) to 3 (strong
100 GUS signal in vasculature and neighboring leaf tissues). To quantify the effect of flg22 on root
101 meristems, seedlings were germinated in liquid MS as per (Luna et al., 2011). Liquid medium was
102 refreshed after one week of growth, and flg22 treatments applied one day later. Mock treatments (water)
103 or flg22 treatments (1 µM flg22 in water) were applied in the evening of the 8th day, and seedlings
104 processed for microscopy the following day after approximately 20h of treatment. Quantification of *IDA*
105 induction in root meristems was conducted by producing maximum intensity projections of the H2B-
106 TdTomato channel images, and counting the total number of fluorescent nuclei in the meristematic
107 region using the StarDist plugin in ImageJ with predetermined settings (Schmidt et al., 2018). To assay
108 the responsiveness of AZs to flg22, plants were grown to maturity in standard conditions. Developing
109 siliques in positions 6-7 that had already shed all floral organs were selected and separated from the
110 plant by the pedicel. The siliques were immediately submerged in the mock (water with 0.02% Silwet
111 L-77) or flg22 treatments (10 µM flg22, 0.02% Silwet L-77 in water) for 15 minutes. Subsequently, the
112 siliques were transferred to the overnight incubation solutions for mock (water) or flg22 treatments (10
113 nM flg22 in water). The initial short treatment with detergent allows for the explants to become less
114 hydrophobic and an even elicitation. Incubation overnight in the solutions without detergent helps avoid
115 toxicity. Cauline leaf elicitation with flg22 was conducted on five-week-old plants grown under standard
116 conditions. The first two cauline leaves of each plant were syringe-infiltrated with mock solution (water)
117 or flg22 solution (1 µM flg22 in water). The entire surface of the leaf was infiltrated, including the
118 boundary between leaf and stem. The treatment was allowed to proceed for 20h. The cauline leaf-stem
119 boundary was manually dissected with a razor blade and imaged with confocal microscopy immediately
120 after.

121 *Nicotiana benthamiana* plants were grown in growth chambers with a long day photoperiod, diurnal
122 temperature of 22ºC and night temperature of 19ºC, 150-180 $\mu mol \cdot m^{-2} \cdot s^{-1}$ of light, and 60% relative
123 humidity.

124 **Generation of genetic constructs and transgenic lines**

125 Arabidopsis plants were transformed with Agrobacterium C58 following the floral dip method (Clough
126 and Bent, 1998).

127 Most genetic constructs used in this study were generated with Invitrogen Gateway recombination
128 cloning. Promoter sequences were cloned into the cloning vector pENTR5' (TOPO-TA cloning;
129 Invitrogen). The *IDA* promoter was cloned from C24 gDNA as the 1417bp between the *IDA* translation
130 initiation site (TIS) and the upstream gene *AT1G68780*. *IDA* promoter sequences in C24 and Col-0
131 accessions are identical, with the exception of the length of a dinucleotide repeat located 144bp from
132 the TIS that is extended by 12bp (CACACACACAAG) in the C24 genome. In all other cloning
133 instances, the Col-0 accession was used as template. The *ERF*(-) and *WRKY*(-) versions of the *IDA*
134 promoter were generated by site-directed mutagenesis (Zheng et al., 2004). Five consecutive rounds of
135 site-directed mutagenesis were necessary to generate the *WRKY*(-) *IDA* promoter. The *IDL1* promoter
136 comprises 1557bp between its TSS and the gene upstream AT3G25660. The IDL2 promoter comprises
137 2084bp upstream of its TIS. The *IDL3* promoter comprises 1974bp upstream of its TIS. *WRKY57*
138 promoter covers 2071bp upstream of its TIS. *WRKY60* promoter comprises the 1512bp between its TIS
139 and the upstream gene *AT2G24990*. The *HAESA* promoter contains 1729bp upstream of the 37th bp from
140 the TIS. Coding sequences to be expressed *in planta* were cloned into pDONR221 or pDONR-Zeo in
141 BP Clonase II reactions (Invitrogen). Intronless coding sequences from *IDA*, *WRKY57* and *WRKY60*
142 were PCR amplified from floral tissue cDNA – see the RT-qPCR section for methods regarding RNA
143 extraction and cDNA synthesis. The WRKY57srdx entry vector was obtained by amplifying *WRKY57*
144 coding sequence from floral cDNA using a modified reverse primer containing the coding sequence of
145 the repressor motif SRDX (CTCGATCTGGATCTAGAACTCCGTTTGGGTTTCGCT) in frame with

146 the C-terminus of *WRKY57*. These and entry vectors were recombined into destination vectors from the
147 Nakagawa lab (Nakagawa et al., 2007; Nakagawa et al., 2008; Tanaka et al., 2013) by means of LR
148 recombination reactions using either LR II Clonase or LR II Clonase Plus (Invitrogen). The destination
149 vector used to generate *GFP-GUS* promoter reporter lines was R4L1pGWB632. Luciferase promoter
150 reporters were generated with the destination vector R4L1pGWB635. GFP-tagged translational fusion
151 reporters were cloned into R4pGWB504. Non C-terminally tagged *promoter*:*cds* constructs were cloned
152 into R4pGWB501. Effector constructs to overexpress TFs or negative controls in luciferase assays were
153 cloned into pGWB518.

154 To generate nuclear fluorescent promoter reporters *H2B-TdTomato* and *Venus-H2B*, a pDONR221 entry
155 clone containing the coding sequence of the fusion proteins H2B-TdTomato or Venus-H2B were first
156 generated. The *H2B-TdTomato* sequence was PCR amplified from pAH21-H2B-TdTomato, while the
157 *Venus-H2B* sequence was amplified from pAB146 (kindly provided by Simon Rüdiger). These entry
158 clones were subsequently recombined with the corresponding promoter and/or destination vectors.

159 Col-0 wild-type plants were gene edited to produce the *idl2CR* and *idl3CR* lines with the plasmid system
160 by Fauser et al. comprising pDe-Cas9 and pEn-Chimera vectors (Fauser et al., 2014). Guide RNA
161 protospacers targeting *IDL2* in its 69th codon (BmgBI restriction site), and *IDL3* in its 37th codon (XmnI
162 restriction site) were designed. Transformants were screened by CAPS and mutant alleles confirmed by
163 Sanger sequencing. A +1bp insertion causes a frameshift immediately prior to the IDL2 peptide in
164 *idl2CR* plants, whereas in *idl3CR* plants a -1bp deletion causes a frameshift in the variable region of the
165 IDL3 protein. The Cas9 T-DNA cassette was segregated away from the plant genetic background and
166 homozygous plants for the *idl2CR* or *idl3CR* mutations were confirmed by CAPS and sequencing.

167 Constructs used in the yeast one-hybrid (Y1H) assay were generated by recombining in Gateway LR
168 reactions the *IDA* promoter entry vector with the two yeast reporter plasmids - pMW2 and pMW3
169 (Deplancke et al., 2006) - containing respectively HIS3 or LacZ reporter genes.

170 Primers used to generate these constructs can be found in the Supplemental Table S1.

171 **Detection and visualization of expression reporters**

172 Promoter activity in beta-glucuronidase (GUS; (Jefferson et al., 1987)) reporter lines was detected as
173 follows: explants/seedlings were incubated in ice-cold 90% acetone for 20 minutes, washed for 20
174 minutes in staining buffer without X-Gluc (50 mM $NaPO_4$ pH 7.4, 2 mM potassium ferro-cyanide, 2
175 mM potassium ferri-cyanide, 0.1% Triton X-100), and stained in staining buffer with 2 mM X-Gluc at
176 37ºC for 3h or overnight. The chlorophyll was then cleared from the tissues with washes in 75% ethanol
177 for 1-3 days and imaged on a stereomicroscope or widefield microscope.

178 Fluorescent reporter detection was conducted on live tissue. Explants were mounted in water and
179 immediately imaged in a Zeiss LSM880 confocal microscope. To visualize GFP-tagged translational
180 fusions as well as the GFP-GUS dual reporter or Venus-H2B, fluorophores were excited with a laser
181 wavelength of 488nm. Nuclear transcriptional reporters H2B-TdTomato were excited with a wavelength
182 of 561nm. To colocalize nuclear reporters (GFP or H2B-TdTomato) with 4′,6-diamidino-2-phenylindole
183 (DAPI), live explants were incubated in DAPI staining solution (0.2 mg/L in water) for 30 min and
184 subsequently imaged with an excitation wavelength of 405nm. Chlorophyll autofluorescence was
185 excited with a laser wavelength of 633 nm to allow easier identification of AZ or cauline leaf regions.

186 **AZ and cell size estimations**

187 AZs of six-week-old plants grown in standard conditions were imaged in a stereomicroscope. The
188 transversal area occupied by the receptacle was manually selected in ImageJ (Schneider et al., 2012),
189 and then measured. To estimate the cell size in AZs, the AZs were stained with propidium iodide (10
190 mg/L in water) and imaged in a Zeiss LSM880 confocal microscope with laser excitation at 561nm.
191 Concomitantly, the GFP-tagged proteins were imaged with excitation wavelength of 488nm. For each

192 AZ, the longest possible diameter of five consecutive cells from the sepal AZ were measured manually
193 with ImageJ and then averaged to produce the mean estimated cell size of an AZ. Transversal AZ area
194 was measured in position 12 siliques. Cell size was measured in position 8. These positions displayed
195 the greatest contrast in size between wild-type plants and genotypes in which AZs enlarged, while
196 technically allowing the imaging to be conducted reliably.

197 **Gene expression estimations by RT-qPCR**

198 Floral receptacles were manually dissected from at least 25 flowers (positions five/six) collected from
199 three to four plants to yield each biological replicate. Excised receptacles were immediately transferred
200 to tubes pre-chilled in liquid nitrogen, and flash-frozen in liquid nitrogen. RNA was extracted using
201 either Spectrum Plant Total RNA Kit (Sigma) or RNeasy Plant Mini Kit (Qiagen) following the
202 manufacturer instructions and including an on-column DNase I digestion step (Sigma). First strand
203 cDNA was synthesized with Superscript III or Superscript IV Reverse Transcriptase (Invitrogen), RNA
204 digested with RNase H, and selected loci amplified and quantified with FastStart Essential DNA Green
205 Master (Roche) in a LightCycler96 instrument (Roche). Gene expression was estimated with the $2^{-\Delta Ct}$
206 method using *ACTIN2* as a reference gene. Experiments comprised three biological replicas per
207 genotype and two technical replicas per RT-qPCR reaction. Primers used in RT-qPCR reactions can be
208 found in the Supplemental Table S1.

209 **Luciferase promoter transactivation assays**

210 Transactivation assays in transiently transformed *N. benthamiana* plants were carried out as per
211 (Lasierra and Prat, 2018). Briefly, fully expanded leaves from four-week-old plants were syringe-
212 infiltrated with Agrobacterium solutions carrying the reporter and effector plasmids at 0.02 OD_{600} each.
213 Measurements were conducted three days after infiltration on a 96-well OptiPlate (PerkinElmer) by
214 floating 4 mm diameter leaf discs (abaxial side up) on 200 µL of luciferin solution (1xMS salts, 0.5%
215 MES, pH 5.8, 12 µM D-luciferin). Light emission was measured in a Wallac 1420 VICTOR2 microplate
216 reader (PerkinElmer) recording the light emitted for 10 seconds, with 10 minutes delay between each
217 repeat. The third plate repeat after approximately 35 minutes typically recorded the strongest signal and
218 was used to plot and analyze differences between constructs. Twelve leaf discs per construct
219 combination coming from two different plants per construct combination were assayed per experiment.

220 Assays with the *IDA* promoter luciferase constructs were first attempted in *N. benthamiana* leaves but
221 strong autoactivation of the *IDA* promoter in this system impeded reliable quantifications. An
222 Arabidopsis mesophyll protoplast transient transfection system was used instead. We used fully
223 expanded rosette leaves from pre-bolting, four-week-old Col-0 plants grown in our standard conditions
224 to extract the protoplasts following the tape-sandwich method (Wu et al., 2009; Hansen and van Ooijen,
225 2016). Transfections were carried out with 50 µL of protoplasts at 400000 protoplasts/mL and 6 µg of
226 plasmid DNA, purified with PureLink HiPure Plasmid Midiprep Kit (Thermofisher). After transfections,
227 protoplasts were allowed to recover in W5 solution overnight. The protoplasts were gently pelleted and
228 resuspended in 100 µL of W5 solution with 1 mM D-luciferin and immediately transferred to 96-well
229 plates. Light emission was recorded in for five seconds, with eight minutes delay between each repeat.
230 Four independent protoplast transfections per construct combination were analyzed per experiment.

231 ***In silico* analyses of promoter sequences**

232 The promoter sequence of *IDA* was scouted for presence of TFBSs using Binding Site Prediction tool
233 from the Gao lab's PlantRegMap site (http://plantregmap.gao-lab.org/; Supplemental Table S2; (Tian et
234 al., 2019)). Gene ontology term enrichment analysis was carried out using the GO Term Enrichment
235 tool in PlantRegMap. The input was the list of TFs identified as *IDA* promoter interactors in either HIS3
236 or LacZ assays, and the reference set of genes was the total list of TFs from Arabidopsis thaliana –
237 downloaded from the PlantRegMap site. This tool calculates statistically significant enrichment with
238 topGO and Fisher's exact tests, with threshold p-value $\leq$ 0.01. Additional TFBS searches were

239 conducted with the PlantPAN 3.0 web tool (http://plantpan.itps.ncku.edu.tw/plantpan4; (Chow et al.,
240 2019)).

241 **Yeast one hybrid screen**

242 The *IDA* promoter was recombined in the pMW2 and pMW3 plasmids, respectively, to drive expression
243 of the HIS3 and LACZ reporters (Gaudinier et al., 2017). These reporter plasmids were transformed into
244 the yeast YM4271 strain and the yeast colonies were screened for autoactivation and the construct
245 presence via PCR genotyping. The Enhanced Yeast One-Hybrid screening of the *IDA* promoter against
246 a complete collection of 2000 Arabidopsis transcription factors was done as described previously
247 (Gaudinier et al., 2011; Pruneda-Paz et al., 2014; Gaudinier et al., 2017). The positive interactions were
248 recorded for LacZ and HIS3 activity. The Yeast One-Hybrid screening was carried out by the Yeast One
249 Hybrid Services Core at the UC Davis Genome Center, at the University of California, Davis
250 (https://genomecenter.ucdavis.edu/yeast-one-hybrid-services). Y1H screening results are listed in the
251 Supplemental Table S3.

252 **Floral organ retention quantification**

253 To phenotype and quantify abscission, plants were grown in individual pots and plants from different
254 genotypes shuffled in their positions across the growth tables to minimize positional effects. Plants were
255 grown undisturbed and untouched to minimize uneven shedding of floral organs prior to phenotyping.
256 Phenotyping was generally conducted at week 6 when inflorescences had produced between 20-25
257 flowers post anthesis. Floral organ abscission was quantified by counting the floral organs attached to
258 the flowers in the main inflorescence as per (Alling and Galindo-Trigo, 2023). The main inflorescence
259 stem was shaken four times and the number of floral organs that remained attached to each floral position
260 (P1-P20) was visually inspected.

261 **Results**

262 **Dissection of promoter cis elements suggests the *IDA* gene is subject to intricate transcriptional**
263 **regulation**

264 One of the main genomic features that dictate the expression profile of a gene is the presence of cis
265 regulatory sequences to which TFs specifically bind (TF binding sites (TFBSs)). We used the web based
266 PlantTFDB 4.0 database to determine the presence of conserved TFBSs in the promoter of *IDA* to
267 investigate the determinants of its transcriptional regulation (Jin et al., 2017). We detected TFBSs for
268 all the major TF families in plants, including ethylene-response factor (ERF), and WRKY, among others
269 (Supplemental Figure S1 and Supplemental Table S2). The majority of the TF families detected
270 presented one or more TFBSs within 500 nucleotides of the translation initiation site (TIS) of *IDA*, the
271 portion of promoters shown to withstand the most stringent evolutionary constraints in a panel of
272 Arabidopsis accessions (Korkuc et al., 2014). This suggests the transcription of *IDA* may be effectively
273 controlled by an extensive array of TFs, allowing for its spatially and temporally-restricted, yet highly
274 environmentally-responsive expression pattern (Butenko et al., 2003; Butenko et al., 2006; Vie et al.,
275 2015; Patharkar and Walker, 2016; Lalun et al., 2023).

276 Given the extensive list of potentially important TFBSs (Supplemental Table S2), we decided to conduct
277 proof-of-concept experiments on ERF and WRKY binding sites to functionally demonstrate the
278 physiological relevance of TFBSs for *IDA* expression. Members of the ERF and WRKY TF regulate
279 physiological processes adjacent to *IDA* signaling and abscission such as ethylene signaling, drought
280 responses, MAMP-induced responses, or senescence (Lorenzo et al., 2003; Zhou et al., 2011; Jiang et
281 al., 2012; Chang et al., 2013; Cheng et al., 2013; Lyons et al., 2013; He et al., 2016; Jiang and Yu, 2016;
282 Lal et al., 2018). We used site-directed mutagenesis to disrupt selected TFBSs for ERFs and WRKYs in
283 the *IDA* promoter, and observed the effect of the mutations on the expression of the promoter with a
284 GUS-GFP dual reporter in stably transformed Arabidopsis plants (Tanaka et al., 2013). Disruption of a

285 single ERF TFBS predicted to convey signals of up to 66 ERF TFs was sufficient to reduce the activity
286 of the *IDA* promoter to barely detectable levels in AZs and floral organs (*ERF*(-); Figure 1A, B and
287 Supplemental Figure S2). The *ERF*(-) *IDA* promoter was also inactive during lateral root emergence
288 (Supplemental Figure S3A). We then tested its capacity to genetically complement the abscission
289 phenotype of *ida* knock-outs (Butenko et al., 2003; Cho et al., 2008). The *ERF*(-) promoter was unable
290 to revert the abscission phenotype of *ida*, indicating that its weak activity in nectaries does not induce
291 floral organ separation (Figure 1C, Supplemental Figure S4). These results indicate the ERF-mediated
292 signaling is crucial for *IDA* expression and required for abscission to take place. On the other hand,
293 disrupting the three WRKY TFBSs predicted with our initial search did not yield noticeable changes to
294 the promoter activity (Supplemental Figure S1). Additional WRKY TFBSs were found in the *IDA*
295 promoter by alternative bioinformatic tools and a quantifiable decrease in the promoter activity in AZs
296 was observed when five binding sites were mutated (*WRKY*(-); Figure 1A, B and Supplemental Figure
297 S2 and S5; (Chow et al., 2019)). Despite its decreased activity in AZ cells, the *WRKY*(-) *IDA* promoter
298 was still active in floral organs and during lateral root emergence, suggesting that WRKY TFs have an
299 important but not essential role on the developmentally-induced expression of *IDA* (Supplemental
300 Figure 3B).

301 **WRKY binding sites are necessary to activate the *IDA* promoter in response to the immunity**
302 **elicitor flg22**

303 When plants are compromised by infections, organs that would otherwise be retained are abscised to
304 protect the plant (Lahey et al., 2004; Scalschi et al., 2014; Patharkar et al., 2017). It is well established
305 that bacterial and fungal elicitors induce *IDA* expression, however the molecular mechanism driving this
306 transcriptional upregulation is not known (Vie et al., 2015; Lalun et al., 2023). Several WRKY TFs are
307 elicited by MAMPs like flg22, are capable of inducing transcription of defense-related genes, and their
308 overexpression enhances disease resistance (Asai et al., 2002; Navarro et al., 2004; Zipfel et al., 2004;
309 Birkenbihl et al., 2016). We thus hypothesized WRKY TFBSs in the *IDA* promoter could influence its
310 responsiveness to pathogenic cues. Indeed, *WRKY*(-) reporter lines were significantly less responsive
311 than lines with wild-type *IDA* promoter to treatments with flg22 in multiple tissues (Figure 2). Wild-
312 type *IDA* promoter was strongly activated by flg22 in AZ cells, whereas its *WRKY*(-) counterpart only
313 showed a weak induction (Figure 2A and B). In seedlings, the flg22 treatment also induced the *IDA*
314 promoter in the meristematic zone of the main root, while the *WRKY*(-) IDA promoter failed to do so
315 (Figure 2C and D). The same result was observed when fully expanded rosette leaves were infiltrated
316 with flg22, as the observed induction of *IDA* promoter along the leaf midrib was reduced in the *WRKY*(-
317) reporter lines (Figure 2E and F). The receptors of IDA, HAE and HSL2, are involved in pathogen-
318 induced cauline leaf abscission in Arabidopsis (Patharkar et al., 2017). We therefore looked for
319 upregulation of the *IDA* promoter in cauline abscission zones after infiltrating cauline leaves with flg22.
320 We did not detect *IDA* promoter activity in this tissue under our conditions (Supplemental Figure S6).
321 Our results support a role for WRKY TFs in mediating *IDA* expression upon biotic stress. We propose
322 the *IDA* promoter to be a direct target of immunity-activated WRKYs (Asai et al., 2002; Lal et al., 2018).

323 **WRKY57 is a potential regulator of *IDA* transcription**

324 Next, we aimed to identify and functionally characterize WRKYs that regulate *IDA* expression during
325 floral organ abscission. We screened a collection of 2000 TFs of Arabidopsis in a yeast one-hybrid
326 (Y1H) assay to identify those that bound the *IDA* promoter. This screening detected interaction between
327 the *IDA* promoter and 211 TFs, the majority of which belonged to the main TF types predicted with the
328 *in silico* analysis (Figure 3A and Supplemental Figure S1). A gene ontology enrichment analysis of the
329 211 TFs that bind the *IDA* promoter revealed enriched categories expected of abscission-related genes:
330 floral whorl morphogenesis and carpel formation, sugar and carbohydrate-mediated signaling,
331 regulation of ethylene responses, among others (Figure 3B). Twelve WRKYs were detected in the Y1H
332 screening and most of them were induced in abscission zones as abscission progresses (Supplemental
333 Figure S7A). Out of the 12, WRKY57 and WRKY60 were selected as our primary candidates to regulate

334 *IDA* because i) their own upregulation preceded the induction of *IDA*, and ii) *WRKY57* and *WRKY60*
335 had been highlighted in the list of most significantly regulated genes of the AZ transcriptome (Cai and
336 Lashbrook, 2008). Besides, WRKY57 is involved in balancing jasmonic acid and auxin signaling in
337 leaves during senescence, is a negative regulator of biotic stress resistance and its overexpression confers
338 drought tolerance – processes previously linked to IDA signaling and abscission (Jiang et al., 2012;
339 Jiang et al., 2014; Jiang and Yu, 2016; Serrano-Bueno et al., 2022). Similarly, WRKY60 is involved in
340 immunity, and ABA signaling in osmotic and salt stress (Xu et al., 2006; Chen et al., 2010; Liu et al.,
341 2012).

342 To verify the transcriptomic data *in planta*, transcriptional and translational fusion reporter lines were
343 generated. Unexpectedly, the reporter lines of *WRKY60* indicated that both its promoter activity and its
344 protein accumulation take place outside of the AZs, where WRKY60-GFP accumulates in the nucleus
345 (Supplemental Figure S7B, C and S8A). A *wrky60* T-DNA insertion line was phenotyped at the
346 flowering stage and no abscission defect was observed (Supplemental Figure S7D). Based on this set of
347 results, we discarded WRKY60 as a putative regulator of *IDA* in abscission. The promoter of *WRKY57*
348 was active in AZs prior to abscission, and WRKY57-GFP accumulated in the nuclei of AZ cells,
349 supporting a putative role for WRKY57 in regulating *IDA* and abscission (Figure 3C and D, and
350 Supplemental Figure S8B). A single mutant *wrky57* abscised as wild-type however, WRKYs are
351 considered to be largely redundant with other members of their family (Figure 3E; (Du et al., 2023)).
352 Functional redundancy is most common between proteins with the highest homology and thus we
353 generated a double knock-out mutant between *WRKY57* and *WRKY48,* WRKY57's closest homolog in
354 BLAST searches against the Arabidopsis proteome (Altschul et al., 1990; Jiang et al., 2012). A delay in
355 abscission was observed in *wrky57 wrky48* double mutants compared to wild-type, suggestive of a weak
356 abscission defect (Figure 3E and F). It must be noted that *wrky57 wrky48* mutants fail to fully fertilize
357 some of their siliques (Figure 3G), and so caution should be taken when concluding the cause of the
358 abscission delay observed in this double mutant. Collectively, these findings portrayed WRKY57 as a
359 potential regulator of *IDA* and abscission in redundancy with other WRKYs. This prompted us to
360 functionally characterize WRKY57 activity in abscission zones.

361 **Overexpression of *WRKY57* or a *WRKY57* repressor respectively activates or represses floral**
362 **organ abscission**

363 TFs can positively or negatively regulate the transcription of genes. Typically, TFs bind TFBSs in the
364 promoter region of genes, and recruit additional effectors to mediate activation or repression of
365 transcription. WRKY57 was shown to induce or repress jasmonic acid-induced senescence in
366 Arabidopsis leaves by competitively interacting with repressors from the JASMONATE ZIM-DOMAIN
367 (JAZ), or AUX-IAA families, respectively (Jiang et al., 2014). This functional duality indicates that the
368 activity of WRKY57 is likely dependent on the tissue, developmental stage and environmental cues, as
369 does the abundance of interactors and hormones that influence WRKY57. To shed light on the role of
370 WRKY57 during abscission we locally overexpressed *WRKY57* using the *HAE* promoter – highly active
371 during abscission in both residuum and secession cells (Jinn et al., 2000; Lee et al., 2018). Multiple
372 transgenic lines overexpressing WRKY57-GFP in AZs displayed enlargement of the receptacle after
373 abscission, correlating with the transgene level of expression (Figure 4A, B and Supplemental Figure
374 S9A, B). The AZ enlargement was caused by excessive cell expansion, reminiscent of that observed in
375 plants constitutively overexpressing *IDA* (*p35S*::*IDA*; (Stenvik et al., 2006)), and those expressing *IDA*
376 under the *HAE* promoter (*pHAE*::*IDA*; Figure 4C and Supplemental Figure S9C). The excessive cell
377 expansion is likely due to overactive cell separation, as loose cells detach from the AZs of the WRKY57-
378 GFP overexpressing lines when mounting samples for microscopy (Figure 4D).

379 Conversely, we overexpressed in AZs a chimeric WRKY57 fused to the SRDX repressor domain. The
380 addition of the SRDX repressor domain to the C-terminus of a TF drives transcriptional repression of
381 its target genes (Hiratsu et al., 2003; Heyl et al., 2008; Matsui and Ohme-Takagi, 2010; Mahfouz et al.,
382 2012; Cen et al., 2016). Multiple independent lines expressing *WRKY57srdx* under the *HAE* promoter

383 showed mild to very strong retention of floral organs in developing siliques, showing a correlation
384 between transgene expression level and phenotype severity (Figure 4E, F and G). Opposite phenotypic
385 outcomes on abscission when locally overexpressing WRKY57 or WRKY57srdx indicate that this TF
386 acts as a positive regulator at the developmental stage in which AZ cells are competent to abscise. We
387 observed induction and repression of the *IDA* promoter activity in luciferase transient transactivation
388 assays in Arabidopsis leaf mesophyll protoplasts (Supplemental Figure S10A). WRKY57
389 transactivation of *IDA* promoter was shown to be partially dependent on the presence of the five WRKY
390 TFBSs disrupted in the *WRKY*(-) version of this promoter (Supplemental Figure S10B). These results
391 suggest that WRKY57 positively regulates abscission by activating the *IDA* signaling pathway.

392 **Activation of abscission by WRKY57 requires IDA and redundant IDA-like peptides, as well as**
393 **the receptors HAE and HSL2**

394 Next, we explored the epistasis between the *pHAE::WRKY57-GFP* transgene, *IDA*, and *HAE/HSL2*. We
395 crossed the *ida-2* and *hae hsl2* mutants to the single copy line *pHAE::WRKY57-GFP* (line 6), and
396 obtained double homozygous *ida-2 pHAE::WRKY57-GFP* and triple homozygous *hae hsl2*
397 *pHAE::WRKY57-GFP* plants. Microscopic examination of the receptacle and AZ cells confirmed the
398 effect of the local overexpression of *WRKY57* in AZs depends on *IDA* and the receptors *HAE* and *HSL2*
399 (Figure 5A). Plants lacking functional receptors HAE/HSL2 completely suppressed the AZ enlargement
400 and cell expansion phenotypes; however a weak but statistically significant enlargement was observed
401 in the *ida-2 pHAE::WRKY57-GFP* double mutants (Figure 5B). We sought to independently confirm
402 this result by transforming *ida-1* and *ida-2* alleles of *IDA* with the *pHAE::WRKY57-GFP* construct.
403 Multiple independent lines displayed varying degrees of AZ enlargement and the enlargement correlated
404 with a complementation of the abscission defect of *ida*, suggesting that induction of abscission by
405 WRKY57 is only partially dependent on *IDA* while fully dependent on *HAE/HSL2* (Supplemental Figure
406 S11A). We reasoned WRKY57 could also activate HAE/HSL2 via *IDL1*, *IDL2* or *IDL3* – close
407 homologs of *IDA*. These three *IDL* genes contain several WRKY TFBSs in their promoter sequences,
408 were reported to be expressed in floral receptacles, and expected to play a redundant role with *IDA* in
409 abscission (Supplemental Figure S11B; (Vie et al., 2015)). Transcriptional upregulation of *IDA*, *IDL2*
410 and *IDL3* was detected by RT-qPCR analysis from dissected floral receptacles in *pHAE::WRKY57-GFP*
411 lines, and the capacity of WRKY57 to transactivate *IDL* genes was confirmed in transient luciferase
412 assays in *Nicotiana benthamiana* leaves with the *IDL2* promoter (Figure 5C, Supplemental Figure
413 S11C). These findings support a model where WRKY57 works as a positive regulator of abscission by
414 orchestrating the coordinated expression of several redundant IDL peptides to activate the receptors
415 HAE/HSL2.

416 The abscission inducing activity of *IDL1*, *IDL2* and *IDL3* was demonstrated in constitutive
417 overexpression lines (Stenvik et al., 2008). IDL2 and IDL3 were shown to bind with high affinity the
418 complex formed by HAE and SERK extracellular domains, as well as the extracellular domain of HSL1
419 – closest homolog to HAE/HSL2 in Arabidopsis (Roman et al., 2022). Genetic evidence involving *IDL1*,
420 *IDL2* and *IDL3* in floral organ abscission has nevertheless remained elusive. Promoter reporter lines for
421 *IDL1*, *IDL2* and *IDL3* expressing GUS-GFP were generated and their previously reported expression
422 patterns during abscission confirmed (Stenvik et al., 2008; Vie et al., 2015). *IDL1* promoter activity was
423 detected in the secession cells only, while in the case of *IDL2* and *IDL3*, promoter activities were
424 detected in both residuum and secession cell layers (Figure 5D). Gene-edited knock-out lines for *IDL2*
425 and *IDL3* were generated in the Col-0 background with the CRISPR-Cas9 technology, and higher order
426 mutants were obtained by genetic crosses with previously published *idaCR* and *idl1CR* (Shi et al., 2018;
427 Alling and Galindo-Trigo, 2023). The *idaCR* line was used despite the availability of the *ida-2* allele,
428 also in Col-0, due to T-DNA-induced genomic rearrangements in the *ida-2* line that impede obtaining
429 double mutants between *ida* and *idl1* alleles (Alling and Galindo-Trigo, 2023). Developing siliques in
430 the quadruple mutant *idaCR idl1CR idl2CR idl3CR* retained floral organs more strongly than the single
431 *ida* mutant, confirming the genetic redundancy between these IDL peptides as positive regulators of

abscission (Figure 5E, F and Supplemental Figure S12). Based on the cumulative evidence provided here, we propose a model in which WRKY57 modulates the transcription of *IDA* and *IDL* genes to fine-tune the timing of floral organ abscission.

Discussion

The multiplicity of cues affecting abscission and the expansion of TF families in flowering plants make characterizing transcriptional effectors in this process a demanding task. In this study, we show that the transcriptional regulation of *IDA*, one of the main triggers of floral organ abscission, is subject to the control of TFs from the ERF and WRKY families (Figure 1). Using molecular genetics and physiological assays, we showed that the IDA signaling pathway can be activated upon exposure to a bacterial immune elicitor in AZs, and that this activation depends on WRKY TFBSs in the *IDA* promoter (Figure 2). Screening a large collection of TFs in a heterologous system, we identified a list of potential candidates to directly regulate *IDA* expression, and genetically characterized WRKY57 as such (Figure 3, 4 and 5A and B). Finally, by locally overexpressing WRKY57 in AZs we found evidence of coordinated transcriptional regulation of *IDA*, *IDL2* and *IDL3* (Figure 5C). The generation of higher order *ida/idl* mutants confirmed the long-standing hypothesis of functional redundancy among these genes (Figure 5E and F).

ERFs are known to relay the transcriptional signaling induced by ethylene downstream of the master transcriptional regulator ETHYLENE INSENSITIVE3 (EIN3; (Chao et al., 1997; Chang et al., 2013)). Indeed, the result of disrupting one ERF TFBSs in the *IDA* promoter yielded the same expression pattern observed for the wild-type *IDA* promoter in an ethylene insensitive background (Butenko et al., 2006). It is therefore plausible that ethylene has a lead role in activating *IDA* transcription during the developmentally initiated abscission pathway. Especially so when considering the lack of genetic complementation of the abscission phenotype of *ida* mutant plants when *IDA* expression is driven by a promoter that lacks ERF TFBSs (Figure 1C). Interestingly, the master regulator of ethylene EIN3 was identified in the Y1H screening as a TF that binds the *IDA* promoter (Supplemental Table S3). EIN3 upregulates the transcription of its direct targets, providing further support to the model in which *IDA* is activated by ethylene signaling during floral organ abscission (Chang et al., 2013; Meir et al., 2019). Although *IDA* was not detected in the genome-wide screen for EIN3-mediated, ethylene-induced transcriptionally regulated genes in Arabidopsis, developmental or tissue-specific effects could explain its absence, as these experiments were conducted in 3-day old etiolated seedlings (Chang et al., 2013). Dissecting the importance and the mechanism behind the putative two-tiered regulation of *IDA* by EIN3 and ERFs will be the topic of future investigations.

We have shown that residuum cells of recently abscised floral receptacles (positions six or seven) respond to flg22 treatments by upregulating *IDA* (Figure 2A and B). While the fluorescent reporter data suggests residuum cells are particularly responsive to flg22, this responsiveness pattern may not reflect responsivity *per se*, but rather their capacity to uptake the treatment. Residuum cells synthesize a cuticle after abscission takes place, although in the floral positions analyzed here this process may not have concluded, presenting a less hydrophobic exterior and increased permeability. Regardless of the spatial specificity of the response, the responsivity of the *IDA* promoter in residuum cells to biotic stress after organs abscise has interesting implications. Firstly, it reinforces the notion that IDA signaling is activated in response to flg22 in cells destined for separation. Secondly, reactivation of IDA signaling in the cells that control cell separation will likely incur in the activation of a similar set of responses triggered during abscission, as the expression of receptors HAE/HSL2 and other downstream regulators remains active in residuum cells after separation (Cho et al., 2008). Flg22 elicitation of *IDA* expression could induce a protective shedding mechanism that is useful for the plant when still-attached floral organs are infected by bacterial pathogens, similar to pathogen-induced cauline leaf shedding (Patharkar et al., 2017). Alternatively, activating IDA signaling could help residuum cells protect themselves against pathogens by reinforcing the flg22-mediated signaling. When seedlings are exposed to exogenous IDA peptide, defense response marker genes that are typically induced by flg22 like *FLG22-*

481 *INDUCED RECEPTOR-LIKE KINASE1* (*FRK1;* (Asai et al., 2002)) are transcriptionally upregulated.
482 When seedlings are exposed to both IDA and flg22, the expression of these marker genes is upregulated
483 even further (Lalun et al., 2023). This suggests a role for IDA in enhancing the flg22-mediated
484 transcriptional response, something potentially beneficial for residuum cells to protect them as cell
485 separation occurs. There is however conflicting evidence that indicates a negative role during leaf
486 bacterial colonization for the IDA receptors HAE/HSL2 and the related peptide IDL6 (Wang et al.,
487 2017). Understanding the physiological consequence of the molecular signatures triggered by IDA
488 treatments that overlap with immune responses awaits further analyses. AZ-centric physiological studies
489 will provide exciting new insights into the relationship between abscission and immunity.

490 Out of the twelve WRKYs found in the Y1H screen on the *IDA* promoter, there are several good
491 candidates to regulate *IDA* during biotic stress. In ChIP-seq and mass spectrometry analyses of nuclear
492 proteins, Birkenbihl et al. reported the *IDA* promoter-binding TFs WRKY8 and WRKY11 to be both
493 transcriptionally upregulated and to increase in protein abundance upon flg22 treatments (Birkenbihl et
494 al., 2018). WRKY8 was found to execute most of the transcriptional responses in chitin-induced, PBS1-
495 LIKE 19 (PBL19)-mediated immunity. Upon chitin treatments – also known to induce *IDA* expression
496 –, PBL19 accumulates in the nucleus, interacts and phosphorylates WRKY8 which in turn
497 transcriptionally upregulates genes. Transgenic plants expressing a version of PBL19 that constitutively
498 accumulates in the nucleus show a severe autoimmunity phenotype, which is dependent on WRKY8.
499 An RNAseq analysis of the autoimmune PBL19 expressing plants revealed that *HAE*, *IDL6* and *IDL7*
500 were upregulated along with immunity marker genes like *FRK1* – data for the *IDA* gene was
501 unfortunately not available in the dataset (Li et al., 2022). This suggests that upon chitin perception,
502 WRKY8 induces expression of components of the IDA signaling pathway, and quite possibly also *IDA*.
503 Since WRKY8 increases in abundance upon flg22 detection, it is likely that a similar set of genes are
504 upregulated by WRKY8 in the context of flg22 perception; making WRKY8 a prime candidate to
505 mediate the flg22-induced IDA expression. WRKY11, on the other hand, acts as a negative regulator of
506 gene expression and inhibits transcription of genes typically induced in the context of immunity
507 redundantly with WRKY7, WRKY15, WRKY17, WRKY21 and WRKY39. Quintuple mutants *wrky7-*
508 *11-17-21-39* show severe developmental defects and display constitutive upregulation of defense-
509 related genes. An exploration of the RNAseq dataset comparing *wrky7-11-17-21-39* to wild-type
510 confirmed that the IDA signaling pathway is also differentially expressed, with *IDA*, *HAE*, *IDL6* and
511 *IDL7* being upregulated in the quintuple *wrky* mutant (Du et al., 2023). This set of WRKYs likely
512 constitute a negative feedback loop to the defense-induced transcriptional responses in the plant,
513 including components of the IDA signaling pathway.

514 We have genetically characterized WRKY57 as a potential positive regulator of abscission, exerting its
515 transcriptional control on *IDA*, *IDL2* and *IDL3* (Figure 4 and 5). In rosette leaves, WRKY57 can be co-
516 opted by repressors from the jasmonic acid and auxin signaling pathways to respectively induce or
517 repress jasmonic acid-induced senescence (Jiang et al., 2014). Both hormones have important roles in
518 the abscission and senescence of floral organs. While auxin inhibits abscission (Basu et al., 2013),
519 jasmonic acid signaling regulates floral organ senescence and the timing of abscission (Kubigsteltig et
520 al., 1999; Serrano-Bueno et al., 2022). Thus, we speculate that WRKY57 could help orchestrate the
521 coordinated transcriptional regulation of the *IDA* gene from auxin and jasmonic acid signaling pathways
522 to fine tune abscission timing.

523 The regulatory axis described in this study comprising WRKY-IDA signaling-abscission is not
524 exclusive to floral organ abscission in Arabidopsis. Tomato pedicels have been recently shown to utilize
525 a WRKY TF to mediate low light-induced pedicel abscission by regulating tomato *IDL6* gene expression
526 (Li et al., 2021). This demonstrates the tight relationship between transcriptional regulators of the
527 WRKY family and abscission is conserved across plant species and in diverse plant organs.

528 Introducing beneficial traits into crops by targeted genome editing is easier than ever; however, gene
529 functions are normally multifaceted and involved in multiple processes. Our study exemplifies how

530 promoter element modification can be exploited to allow the developmentally encoded expression
531 profile of a gene to proceed, while impairing its responsiveness to stress (Figure 1 and 2). Promoter
532 targeted genome editing approaches therefore show promise in allowing the introduction of beneficial
533 traits like controlled abscission into crops, while minimizing developmental penalties to yield (Liu et
534 al., 2021; Tang and Zhang, 2023; Zhou et al., 2023).

535 **Supplementary data**

536 **Supplemental Table S1.** Primers used in this study.

537 **Supplemental Table S2.** Transcription factor binding site prediction for the *IDA* promoter.

538 **Supplemental Table S3.** Transcription factors identified to bind the *IDA* promoter in the yeast one-
539 hybrid screening.

540 **Supplemental Figure S1.** Transcription factor binding site analysis of the *IDA* promoter sequence in
541 Arabidopsis.

542 **Supplemental Figure S2.** Additional information to main Figure 1B.

543 **Supplemental Figure S3.** Histochemical detection of GUS activity during lateral root emergence.

544 **Supplemental Figure S4.** The *ERF(-)* version of the *IDA* promoter cannot rescue the abscission defect
545 of the *ida-1* mutant.

546 **Supplemental Figure S5.** Deletion of individual WRKY binding sites in the *IDA* promoter does not
547 impair its activity during abscission.

548 **Supplemental Figure S6.** Elicitation of immune responses in cauline leaves with flg22 does not induce
549 *IDA* in the cauline AZ.

550 **Supplemental Figure S7.** Additional information to main Figure 3.

551 **Supplemental Figure S8.** Nuclear localization of the fusion proteins WRKY60-GFP and WRKY57-
552 GFP.

553 **Supplemental Figure S9.** Quantification of the receptacle enlargement phenotype shown in the main
554 Figure 4.

555 **Supplemental Figure S10.** Transient transactivation of the *IDA* promoter by WRKY57 in Arabidopsis
556 mesophyll protoplasts.

557 **Supplemental Figure S11**. WRKY57 activates the abscission pathway in *ida* mutants via *IDL* peptides.

558 **Supplemental Figure S12.** Quantification of floral organ abscission at positions 8, 10, 12, 16 and 20.

559 **Acknowledgements**

560 The authors thank Prof. Dr. Reidunn Aallen for sharing the *idl1CR*, *idl2CR* and *idl3CR* lines; Prof. Dr.
561 Rüdiger Simon for sharing the H2B-TdTomato plasmid; and Verena Mertes for her initial contributions
562 to the Y1H screening. We thank the NorMic microscopy platform for their help and support. We thank
563 the technician team at EVOGENE for their technical support.

564 **Author contributions**

565 S.G-T. conceived and developed the research hypotheses, produced the genetic materials, carried out
566 the experimentation, data analyses and interpretation, wrote the manuscript and prepared all figures and
567 illustrations. T.I. and S.S. provided the *idl2CR* and *idl3CR* lines. A-M.B. cloned the Y1H constructs and
568 carried out the Y1H screen together with S.B. M.A.B. designed the Y1H screen of the *IDA* promoter

with S.B., acquired funding, administered resources, and provided initial guidance interpreting the abscission phenotypes. All authors read the manuscript and provided feedback.

Conflict of interest

The authors have no conflicts of interest to declare.

Funding

Funding to S.G-T. was kindly provided through the Norwegian Ministry of Education and Research and by the Department of Biosciences, University of Oslo. Funding was also provided through the Research Council of Norway (grant 230849) to S.G-T. and M.A.B. A-M.B. was partially supported by the UC Davis Genome Center. S.M.B. was supported by an HHMI Faculty fellowship and the yeast one hybrid assay development by NSF-MCB-1330337.

Data availability

All data presented can be found in the manuscript and supplementary data. Requests for further details can be directed to the corresponding authors.

References

Abeles F, Rubinstein B (1964) Regulation of ethylene evolution and leaf abscission by auxin. Plant Physiology **39:** 963

Addicott F, Lynch R, Carns H (1955) Auxin gradient theory of abscission regulation. Science **121:** 644-645

Alling R, Galindo-Trigo S (2023) Reproductive defects in the abscission mutant ida-2 are caused by T-DNA induced genomic rearrangements. Plant Physiol

Aloni B, Karni L, Zaidman Z, Schaffer AA (1997) The Relationship between Sucrose Supply, Sucrose-cleaving Enzymes and Flower Abortion in Pepper. Annals of Botany **79:** 601-605

Altschul SF, Gish W, Miller W, Myers EW, Lipman DJ (1990) Basic local alignment search tool. Journal of Molecular Biology **215:** 403-410

Asai T, Tena G, Plotnikova J, Willmann MR, Chiu W-L, Gomez-Gomez L, Boller T, Ausubel FM, Sheen J (2002) MAP kinase signalling cascade in Arabidopsis innate immunity. Nature **415:** 977-983

Baer J, Taylor I, Walker JC (2016) Disrupting ER-associated protein degradation suppresses the abscission defect of a weak hae hsl2 mutant in Arabidopsis. Journal of Experimental Botany **67:** 5473-5484

Basu MM, González-Carranza ZH, Azam-Ali S, Tang S, Shahid AA, Roberts JA (2013) The Manipulation of Auxin in the Abscission Zone Cells of Arabidopsis Flowers Reveals That Indoleacetic Acid Signaling Is a Prerequisite for Organ Shedding Plant Physiology **162:** 96-106

Ben-David A, Bashan Y, Okon Y (1986) Ethylene production in pepper (Capsicum annuum) leaves infected with Xanthomonas campestris pv. vesicatoria. Physiological and Molecular Plant Pathology **29:** 305-316

Birkenbihl RP, Kracher B, Roccaro M, Somssich IE (2016) Induced Genome-Wide Binding of Three Arabidopsis WRKY Transcription Factors during Early MAMP-Triggered Immunity. The Plant Cell **29:** 20-38

Birkenbihl RP, Kracher B, Ross A, Kramer K, Finkemeier I, Somssich IE (2018) Principles and characteristics of the Arabidopsis WRKY regulatory network during early MAMP-triggered immunity. The Plant Journal **96:** 487-502

Botton A, Ruperti B (2019) The Yes and No of the Ethylene Involvement in Abscission. Plants **8:** 187

Brown KM (1997) Ethylene and abscission. Physiologia Plantarum **100:** 567-576

Burg SP (1968) Ethylene, plant senescence and abscission. Plant Physiol **43:** 1503-1511

Burr CA, Leslie ME, Orlowski SK, Chen I, Wright CE, Daniels MJ, Liljegren SJ (2011) CAST AWAY, a Membrane-Associated Receptor-Like Kinase, Inhibits Organ Abscission in Arabidopsis Plant Physiology **156:** 1837-1850

Butenko MA, Patterson SE, Grini PE, Stenvik GE, Amundsen SS, Mandal A, Aalen RB (2003) Inflorescence deficient in abscission controls floral organ abscission in Arabidopsis and identifies a novel family of putative ligands in plants. Plant Cell **15:** 2296-2307

Butenko MA, Shi C-L, Aalen RB (2012) KNAT1, KNAT2 and KNAT6 act downstream in the IDA-HAE/HSL2 signaling pathway to regulate floral organ abscission. Plant Signaling & Behavior **7:** 135-138

Butenko MA, Stenvik GE, Alm V, Saether B, Patterson SE, Aalen RB (2006) Ethylene-dependent and -independent pathways controlling floral abscission are revealed to converge using promoter::reporter gene constructs in the ida abscission mutant. J Exp Bot **57:** 3627-3637

Cai S, Lashbrook CC (2008) Stamen Abscission Zone Transcriptome Profiling Reveals New Candidates for Abscission Control: Enhanced Retention of Floral Organs in Transgenic Plants Overexpressing Arabidopsis ZINC FINGER PROTEIN2 Plant Physiology **146:** 1305-1321

Cen H, Ye W, Liu Y, Li D, Wang K, Zhang W (2016) Overexpression of a Chimeric Gene, OsDST-SRDX, Improved Salt Tolerance of Perennial Ryegrass. Scientific Reports **6:** 27320

Chang KN, Zhong S, Weirauch MT, Hon G, Pelizzola M, Li H, Huang S-sC, Schmitz RJ, Urich MA, Kuo D, Nery JR, Qiao H, Yang A, Jamali A, Chen H, Ideker T, Ren B, Bar-Joseph

Z, Hughes TR, Ecker JR (2013) Temporal transcriptional response to ethylene gas drives growth hormone cross-regulation in Arabidopsis. eLife **2:** e00675

Chao Q, Rothenberg M, Solano R, Roman G, Terzaghi W, Ecker† JR (1997) Activation of the Ethylene Gas Response Pathway in Arabidopsis by the Nuclear Protein ETHYLENE-INSENSITIVE3 and Related Proteins. Cell **89:** 1133-1144

Chen H, Lai Z, Shi J, Xiao Y, Chen Z, Xu X (2010) Roles of arabidopsis WRKY18, WRKY40 and WRKY60 transcription factors in plant responses to abscisic acid and abiotic stress. BMC Plant Biology **10:** 281

Cheng M-C, Liao P-M, Kuo W-W, Lin T-P (2013) The Arabidopsis ETHYLENE RESPONSE FACTOR1 Regulates Abiotic Stress-Responsive Gene Expression by Binding to Different cis-Acting Elements in Response to Different Stress Signals Plant Physiology **162:** 1566-1582

Cho SK, Larue CT, Chevalier D, Wang H, Jinn T-L, Zhang S, Walker JC (2008) Regulation of floral organ abscission in Arabidopsis thaliana. Proceedings of the National Academy of Sciences **105:** 15629-15634

Chow CN, Lee TY, Hung YC, Li GZ, Tseng KC, Liu YH, Kuo PL, Zheng HQ, Chang WC (2019) PlantPAN3.0: a new and updated resource for reconstructing transcriptional regulatory networks from ChIP-seq experiments in plants. Nucleic Acids Res **47:** D1155-D1163

Cin VD, Danesin M, Boschetti A, Dorigoni A, Ramina A (2005) Ethylene biosynthesis and perception in apple fruitlet abscission (Malus domestica L. Borck). Journal of Experimental Botany **56:** 2995-3005

Clough SJ, Bent AF (1998) Floral dip: a simplified method for Agrobacterium -mediated transformation of Arabidopsis thaliana. The Plant Journal **16:** 735-743

Crick J, Corrigan L, Belcram K, Khan M, Dawson JW, Adroher B, Li S, Hepworth SR, Pautot V (2022) Floral organ abscission in Arabidopsis requires the combined activities of three TALE homeodomain transcription factors. Journal of Experimental Botany **73:** 6150-6169

Deplancke B, Mukhopadhyay A, Ao W, Elewa AM, Grove CA, Martinez NJ, Sequerra R, Doucette-Stamm L, Reece-Hoyes JS, Hope IA, Tissenbaum HA, Mango SE, Walhout AJM (2006) A Gene-Centered C. elegans Protein-DNA Interaction Network. Cell **125:** 1193-1205

Du P, Wang Q, Yuan D-Y, Chen S-S, Su Y-N, Li L, Chen S, He X-J (2023) WRKY transcription factors and OBERON histone-binding proteins form complexes to balance plant growth and stress tolerance. The EMBO Journal **n/a:** e113639

Elmo M. Beyer, Jr., Morgan PW (1971) Abscission: The Role of Ethylene Modification of Auxin Transport. Plant Physiology **48:** 208-212

Fauser F, Schiml S, Puchta H (2014) Both CRISPR/Cas-based nucleases and nickases can be used efficiently for genome engineering in Arabidopsis thaliana. The Plant Journal **79:** 348-359

Gaudinier A, Tang M, Bågman A-M, Brady SM (2017) Identification of Protein–DNA Interactions Using Enhanced Yeast One-Hybrid Assays and a Semiautomated Approach. *In* W Busch, ed, Plant Genomics: Methods and Protocols. Springer New York, New York, NY, pp 187-215

Gaudinier A, Zhang L, Reece-Hoyes JS, Taylor-Teeples M, Pu L, Liu Z, Breton G, Pruneda-Paz JL, Kim D, Kay SA, Walhout AJM, Ware D, Brady SM (2011) Enhanced Y1H assays for Arabidopsis. Nature Methods **8:** 1053-1055

Glick E, Levy Y, Gafni Y (2009) The viral etiology of tomato yellow leaf curl disease–a review. Plant Protection Science **45:** 81-97

Gubert CM, Liljegren SJ (2014) HAESA and HAESA-LIKE2 activate organ abscission downstream of NEVERSHED and EVERSHED in Arabidopsis flowers. Plant Signaling & Behavior **9:** e29115

Hansen LL, van Ooijen G (2016) Rapid Analysis of Circadian Phenotypes in Arabidopsis Protoplasts Transfected with a Luminescent Clock Reporter. JoVE**:** e54586

He G-H, Xu J-Y, Wang Y-X, Liu J-M, Li P-S, Chen M, Ma Y-Z, Xu Z-S (2016) Drought-responsive WRKY transcription factor genes TaWRKY1 and TaWRKY33 from wheat confer drought and/or heat resistance in Arabidopsis. BMC Plant Biology **16:** 116

Heyl A, Ramireddy E, Brenner WG, Riefler M, Allemeersch J, Schmülling T (2008) The Transcriptional Repressor ARR1-SRDX Suppresses Pleiotropic Cytokinin Activities in Arabidopsis Plant Physiology **147:** 1380-1395

Hiratsu K, Matsui K, Koyama T, Ohme-Takagi M (2003) Dominant repression of target genes by chimeric repressors that include the EAR motif, a repression domain, in Arabidopsis. The Plant Journal **34:** 733-739

Jefferson RA, Kavanagh TA, Bevan MW (1987) GUS fusions: beta-glucuronidase as a sensitive and versatile gene fusion marker in higher plants. The EMBO Journal **6:** 3901-3907

Jiang Y, Liang G, Yang S, Yu D (2014) Arabidopsis WRKY57 Functions as a Node of Convergence for Jasmonic Acid– and Auxin-Mediated Signaling in Jasmonic Acid–Induced Leaf Senescence. The Plant Cell **26:** 230-245

Jiang Y, Liang G, Yu D (2012) Activated Expression of WRKY57 Confers Drought Tolerance in Arabidopsis. Molecular Plant **5:** 1375-1388

Jiang Y, Yu D (2016) The WRKY57 Transcription Factor Affects the Expression of Jasmonate ZIM-Domain Genes Transcriptionally to Compromise Botrytis cinerea Resistance. Plant Physiology **171:** 2771-2782

Jin J, Tian F, Yang DC, Meng YQ, Kong L, Luo J, Gao G (2017) PlantTFDB 4.0: toward a central hub for transcription factors and regulatory interactions in plants. Nucleic Acids Res **45:** D1040-D1045

Jinn T-L, Stone JM, Walker JC (2000) HAESA, an Arabidopsis leucine-rich repeat receptor kinase, controls floral organ abscission. Genes & Development **14:** 108-117

Ketring DL, Melouk HA (1982) Ethylene Production and Leaflet Abscission of Three Peanut Genotypes Infected with Cercospora arachidicola Hori 1 2. Plant Physiology **69:** 789-792

Korkuc P, Schippers JH, Walther D (2014) Characterization and identification of cis-regulatory elements in Arabidopsis based on single-nucleotide polymorphism information. Plant Physiol **164:** 181-200

Kubigsteltig I, Laudert D, Weiler EW (1999) Structure and regulation of the Arabidopsis thaliana allene oxide synthase gene. Planta **208:** 463-471

Lahey KA, Yuan R, Burns JK, Ueng PP, Timmer LW, Chung K-R (2004) Induction of Phytohormones and Differential Gene Expression in Citrus Flowers Infected by the Fungus Colletotrichum acutatum. Molecular Plant-Microbe Interactions® **17:** 1394-1401

Lal NK, Nagalakshmi U, Hurlburt NK, Flores R, Bak A, Sone P, Ma X, Song G, Walley J, Shan L, He P, Casteel C, Fisher AJ, Dinesh-Kumar SP (2018) The Receptor-like Cytoplasmic Kinase BIK1 Localizes to the Nucleus and Regulates Defense Hormone Expression during Plant Innate Immunity. Cell Host & Microbe **23:** 485-497.e485

Lalun VO, Breiden M, Galindo-Trigo S, Smakowska-Luzan E, Simon R, Butenko MA (2023) A dual function of the IDA peptide in regulating cell separation and modulating plant immunity at the molecular level. *In*. eLife Sciences Publications, Ltd

Lasierra P, Prat S (2018) Transient Transactivation Studies in Nicotiana benthamiana Leaves. *In* L Oñate-Sánchez, ed, Two-Hybrid Systems: Methods and Protocols. Springer New York, New York, NY, pp 311-322

Lee Y, Yoon TH, Lee J, Jeon SY, Lee JH, Lee MK, Chen H, Yun J, Oh SY, Wen X, Cho HK, Mang H, Kwak JM (2018) A Lignin Molecular Brace Controls Precision Processing of Cell Walls Critical for Surface Integrity in Arabidopsis. Cell **173:** 1468-1480 e1469

Leslie ME, Lewis MW, Youn J-Y, Daniels MJ, Liljegren SJ (2010) The EVERSHED receptor-like kinase modulates floral organ shedding in Arabidopsis. Development **137:** 467-476

Li R, Shi C-L, Wang X, Meng Y, Cheng L, Jiang C-Z, Qi M, Xu T, Li T (2021) Inflorescence abscission protein SlIDL6 promotes low light intensity-induced tomato flower abscission. Plant Physiology **186:** 1288-1301

Li Y, Xue J, Wang F-Z, Huang X, Gong B-Q, Tao Y, Shen W, Tao K, Yao N, Xiao S, Zhou J-M, Li J-F (2022) Plasma membrane-nucleo-cytoplasmic coordination of a receptor-like cytoplasmic kinase promotes EDS1-dependent plant immunity. Nature Plants **8:** 802-816

Liljegren SJ, Leslie ME, Darnielle L, Lewis MW, Taylor SM, Luo R, Geldner N, Chory J, Randazzo PA, Yanofsky MF, Ecker JR (2009) Regulation of membrane trafficking and organ separation by the NEVERSHED ARF-GAP protein. Development **136:** 1909-1918

Liu B, Butenko MA, Shi C-L, Bolivar JL, Winge P, Stenvik G-E, Vie AK, Leslie ME, Brembu T, Kristiansen W, Bones AM, Patterson SE, Liljegren SJ, Aalen RB (2013) NEVERSHED and INFLORESCENCE DEFICIENT IN ABSCISSION are differentially required for cell

expansion and cell separation during floral organ abscission in Arabidopsis thaliana. Journal of Experimental Botany **64:** 5345-5357

Liu L, Gallagher J, Arevalo ED, Chen R, Skopelitis T, Wu Q, Bartlett M, Jackson D (2021) Enhancing grain-yield-related traits by CRISPR–Cas9 promoter editing of maize CLE genes. Nature Plants **7:** 287-294

Liu Z-Q, Yan L, Wu Z, Mei C, Lu K, Yu Y-T, Liang S, Zhang X-F, Wang X-F, Zhang D-P (2012) Cooperation of three WRKY-domain transcription factors WRKY18, WRKY40, and WRKY60 in repressing two ABA-responsive genes ABI4 and ABI5 in Arabidopsis. Journal of Experimental Botany **63:** 6371-6392

Lorenzo O, Piqueras R, Sánchez-Serrano JJ, Solano R (2003) ETHYLENE RESPONSE FACTOR1 Integrates Signals from Ethylene and Jasmonate Pathways in Plant Defense[W]. The Plant Cell **15:** 165-178

Louie Jr D, Addicott F (1970) Applied auxin gradients and abscission in explants. Plant Physiology **45:** 654

Luna E, Pastor V, Robert J, Flors V, Mauch-Mani B, Ton J (2011) Callose Deposition: A Multifaceted Plant Defense Response. Molecular Plant-Microbe Interactions® **24:** 183-193

Lyons R, Iwase A, Gänsewig T, Sherstnev A, Duc C, Barton GJ, Hanada K, Higuchi-Takeuchi M, Matsui M, Sugimoto K, Kazan K, Simpson GG, Shirasu K (2013) The RNA-binding protein FPA regulates flg22-triggered defense responses and transcription factor activity by alternative polyadenylation. Scientific Reports **3:** 2866

Ma C, Jiang C-Z, Gao J (2021) Regulatory Mechanisms Underlying Activation of Organ Abscission. *In* Annual Plant Reviews online, pp 27-56

Mahfouz MM, Li L, Piatek M, Fang X, Mansour H, Bangarusamy DK, Zhu J-K (2012) Targeted transcriptional repression using a chimeric TALE-SRDX repressor protein. Plant Molecular Biology **78:** 311-321

Matsui K, Ohme-Takagi M (2010) Detection of protein–protein interactions in plants using the transrepressive activity of the EAR motif repression domain. The Plant Journal **61:** 570-578

McKim SM, Stenvik G-E, Butenko MA, Kristiansen W, Cho SK, Hepworth SR, Aalen RB, Haughn GW (2008) The BLADE-ON-PETIOLE genes are essential for abscission zone formation in Arabidopsis. Development **135:** 1537-1546

Meir S, Hunter DA, Chen J-C, Halaly V, Reid MS (2006) Molecular changes occurring during acquisition of abscission competence following auxin depletion in Mirabilis jalapa. Plant Physiology **141:** 1604-1616

Meir S, Philosoph-Hadas S, Riov J, Tucker ML, Patterson SE, Roberts JA (2019) Re-evaluation of the ethylene-dependent and -independent pathways in the regulation of floral and organ abscission. Journal of Experimental Botany **70:** 1461-1467

Meir S, Philosoph-Hadas S, Sundaresan S, Selvaraj KV, Burd S, Ophir R, Kochanek B, Reid MS, Jiang C-Z, Lers A (2010) Microarray analysis of the abscission-related transcriptome in the tomato flower abscission zone in response to auxin depletion. Plant Physiology **154:** 1929-1956

Meir S, Sundaresan S, Riov J, Agarwal I, Philosoph-Hadas S (2015) Role of auxin depletion in abscission control. Stewart Postharvest Rev **11:** 1-15

Meng X, Zhou J, Tang J, Li B, de Oliveira Marcos VV, Chai J, He P, Shan L (2016) Ligand-Induced Receptor-like Kinase Complex Regulates Floral Organ Abscission in Arabidopsis. Cell Reports **14:** 1330-1338

Merelo P, Agustí J, Arbona V, Costa ML, Estornell LH, Gómez-Cadenas A, Coimbra S, Gómez MD, Pérez-Amador MA, Domingo C, Talón M, Tadeo FR (2017) Cell Wall Remodeling in Abscission Zone Cells during Ethylene-Promoted Fruit Abscission in Citrus. Frontiers in Plant Science **8**

Nakagawa T, Nakamura S, Tanaka K, Kawamukai M, Suzuki T, Nakamura K, Kimura T, Ishiguro S (2008) Development of R4 Gateway Binary Vectors (R4pGWB) Enabling High-Throughput Promoter Swapping for Plant Research. Bioscience, Biotechnology, and Biochemistry **72:** 624-629

Nakagawa T, Suzuki T, Murata S, Nakamura S, Hino T, Maeo K, Tabata R, Kawai T, Tanaka K, Niwa Y, Watanabe Y, Nakamura K, Kimura T, Ishiguro S (2007) Improved Gateway

Binary Vectors: High-Performance Vectors for Creation of Fusion Constructs in Transgenic Analysis of Plants. Bioscience, Biotechnology, and Biochemistry **71:** 2095-2100
Navarro L, Zipfel C, Rowland O, Keller I, Robatzek S, Boller T, Jones JDG (2004) The Transcriptional Innate Immune Response to flg22. Interplay and Overlap with Avr Gene-Dependent Defense Responses and Bacterial Pathogenesis Plant Physiology **135:** 1113-1128
Patharkar OR, Gassmann W, Walker JC (2017) Leaf shedding as an anti-bacterial defense in Arabidopsis cauline leaves. PLOS Genetics **13:** e1007132
Patharkar OR, Walker JC (2015) Floral organ abscission is regulated by a positive feedback loop. Proceedings of the National Academy of Sciences **112:** 2906-2911
Patharkar OR, Walker JC (2016) Core Mechanisms Regulating Developmentally Timed and Environmentally Triggered Abscission. Plant Physiol **172:** 510-520
Peng G, Wu J, Lu W, Li J (2013) A polygalacturonase gene clustered into clade E involved in lychee fruitlet abscission. Scientia Horticulturae **150:** 244-250
Pickersgill B (2007) Domestication of Plants in the Americas: Insights from Mendelian and Molecular Genetics. Annals of Botany **100:** 925-940
Pruneda-Paz JL, Breton G, Nagel DH, Kang SE, Bonaldi K, Doherty CJ, Ravelo S, Galli M, Ecker JR, Kay SA (2014) A genome-scale resource for the functional characterization of Arabidopsis transcription factors. Cell reports **8:** 622-632
Reichardt S, Piepho H-P, Stintzi A, Schaller A (2020) Peptide signaling for drought-induced tomato flower drop. Science **367:** 1482-1485
Reid MS (1985) Ethylene and abscission. HortScience **20:** 45-50
Roman A-O, Jimenez-Sandoval P, Augustin S, Broyart C, Hothorn LA, Santiago J (2022) HSL1 and BAM1/2 impact epidermal cell development by sensing distinct signaling peptides. Nature Communications **13:** 876
Santiago J, Brandt B, Wildhagen M, Hohmann U, Hothorn LA, Butenko MA, Hothorn M (2016) Mechanistic insight into a peptide hormone signaling complex mediating floral organ abscission. eLife **5:** e15075
Sawicki M, Aït Barka E, Clément C, Vaillant-Gaveau N, Jacquard C (2015) Cross-talk between environmental stresses and plant metabolism during reproductive organ abscission. Journal of Experimental Botany **66:** 1707-1719
Scalschi L, Camañes G, Llorens E, Fernández-Crespo E, López MM, García-Agustín P, Vicedo B (2014) Resistance Inducers Modulate Pseudomonas syringae pv. Tomato Strain DC3000 Response in Tomato Plants. PLOS ONE **9:** e106429
Schmidt U, Weigert M, Broaddus C, Myers G (2018) Cell Detection with Star-Convex Polygons. *In*. Springer International Publishing, Cham, pp 265-273
Schneider CA, Rasband WS, Eliceiri KW (2012) NIH Image to ImageJ: 25 years of image analysis. Nature Methods **9:** 671-675
Serrano-Bueno G, de los Reyes P, Chini A, Ferreras-Garrucho G, Sánchez de Medina-Hernández V, Boter M, Solano R, Valverde F (2022) Regulation of floral senescence in Arabidopsis by coordinated action of CONSTANS and jasmonate signaling. Molecular Plant **15:** 1710-1724
Shi C-L, Stenvik G-E, Vie AK, Bones AM, Pautot V, Proveniers M, Aalen RB, Butenko MA (2011) Arabidopsis Class I KNOTTED-Like Homeobox Proteins Act Downstream in the IDA-HAE/HSL2 Floral Abscission Signaling Pathway. The Plant Cell **23:** 2553-2567
Shi C-L, von Wangenheim D, Herrmann U, Wildhagen M, Kulik I, Kopf A, Ishida T, Olsson V, Anker MK, Albert M, Butenko MA, Felix G, Sawa S, Claassen M, Friml J, Aalen RB (2018) The dynamics of root cap sloughing in Arabidopsis is regulated by peptide signalling. Nature Plants **4:** 596-604
Stenvik G-E, Butenko MA, Urbanowicz BR, Rose JKC, Aalen RB (2006) Overexpression of INFLORESCENCE DEFICIENT IN ABSCISSION Activates Cell Separation in Vestigial Abscission Zones in Arabidopsis. The Plant Cell **18:** 1467-1476
Stenvik G-E, Tandstad NM, Guo Y, Shi C-L, Kristiansen W, Holmgren A, Clark SE, Aalen RB, Butenko MA (2008) The EPIP Peptide of INFLORESCENCE DEFICIENT IN ABSCISSION Is Sufficient to Induce Abscission in Arabidopsis through the Receptor-Like Kinases HAESA and HAESA-LIKE2 The Plant Cell **20:** 1805-1817

Tanaka Y, Shibahara K, Nakagawa T (2013) Development of Gateway Binary Vectors R4L1pGWB Possessing the Bialaphos Resistance Gene (bar) and the Tunicamycin Resistance Gene as Markers for Promoter Analysis in Plants. Bioscience, Biotechnology, and Biochemistry **77:** 1795-1797

Tang X, Zhang Y (2023) Beyond knockouts: fine-tuning regulation of gene expression in plants with CRISPR-Cas-based promoter editing. New Phytologist **239:** 868-874

Taylor I, Baer J, Calcutt R, Walker JC (2019) Hypermorphic SERK1 Mutations Function via a SOBIR1 Pathway to Activate Floral Abscission Signaling. Plant Physiology **180:** 1219-1229

Tian F, Yang D-C, Meng Y-Q, Jin J, Gao G (2019) PlantRegMap: charting functional regulatory maps in plants. Nucleic Acids Research **48:** D1104-D1113

Vie AK, Najafi J, Liu B, Winge P, Butenko MA, Hornslien KS, Kumpf R, Aalen RB, Bones AM, Brembu T (2015) The IDA/IDA-LIKE and PIP/PIP-LIKE gene families in Arabidopsis: phylogenetic relationship, expression patterns, and transcriptional effect of the PIPL3 peptide. J Exp Bot **66:** 5351-5365

Wang X-Q, XU W-H, Ma L-G, Fu Z-M, Deng X-W, Li J-Y, Wang Y-H (2006) Requirement of KNAT1/BP for the Development of Abscission Zones in Arabidopsis thaliana. Journal of Integrative Plant Biology **48:** 15-26

Wang X, Hou S, Wu Q, Lin M, Acharya BR, Wu D, Zhang W (2017) IDL6-HAE/HSL2 impacts pectin degradation and resistance to Pseudomonas syringae pv tomato DC3000 in Arabidopsis leaves. The Plant Journal **89:** 250-263

Wu F-H, Shen S-C, Lee L-Y, Lee S-H, Chan M-T, Lin C-S (2009) Tape-Arabidopsis Sandwich - a simpler Arabidopsis protoplast isolation method. Plant Methods **5:** 16

Xu X, Chen C, Fan B, Chen Z (2006) Physical and Functional Interactions between Pathogen-Induced Arabidopsis WRKY18, WRKY40, and WRKY60 Transcription Factors. The Plant Cell **18:** 1310-1326

Zheng L, Baumann U, Reymond J-L (2004) An efficient one-step site-directed and site-saturation mutagenesis protocol. Nucleic Acids Research **32:** e115-e115

Zhou J, Liu G, Zhao Y, Zhang R, Tang X, Li L, Jia X, Guo Y, Wu Y, Han Y, Bao Y, He Y, Han Q, Yang H, Zheng X, Qi Y, Zhang T, Zhang Y (2023) An efficient CRISPR–Cas12a promoter editing system for crop improvement. Nature Plants **9:** 588-604

Zhou X, Jiang Y, Yu D (2011) WRKY22 transcription factor mediates dark-induced leaf senescence in Arabidopsis. Molecules and Cells **31:** 303-313

Zhu Q, Shao Y, Ge S, Zhang M, Zhang T, Hu X, Liu Y, Walker J, Zhang S, Xu J (2019) A MAPK cascade downstream of IDA–HAE/HSL2 ligand–receptor pair in lateral root emergence. Nature Plants **5:** 414-423

Zipfel C, Robatzek S, Navarro L, Oakeley EJ, Jones JDG, Felix G, Boller T (2004) Bacterial disease resistance in Arabidopsis through flagellin perception. Nature **428:** 764-767

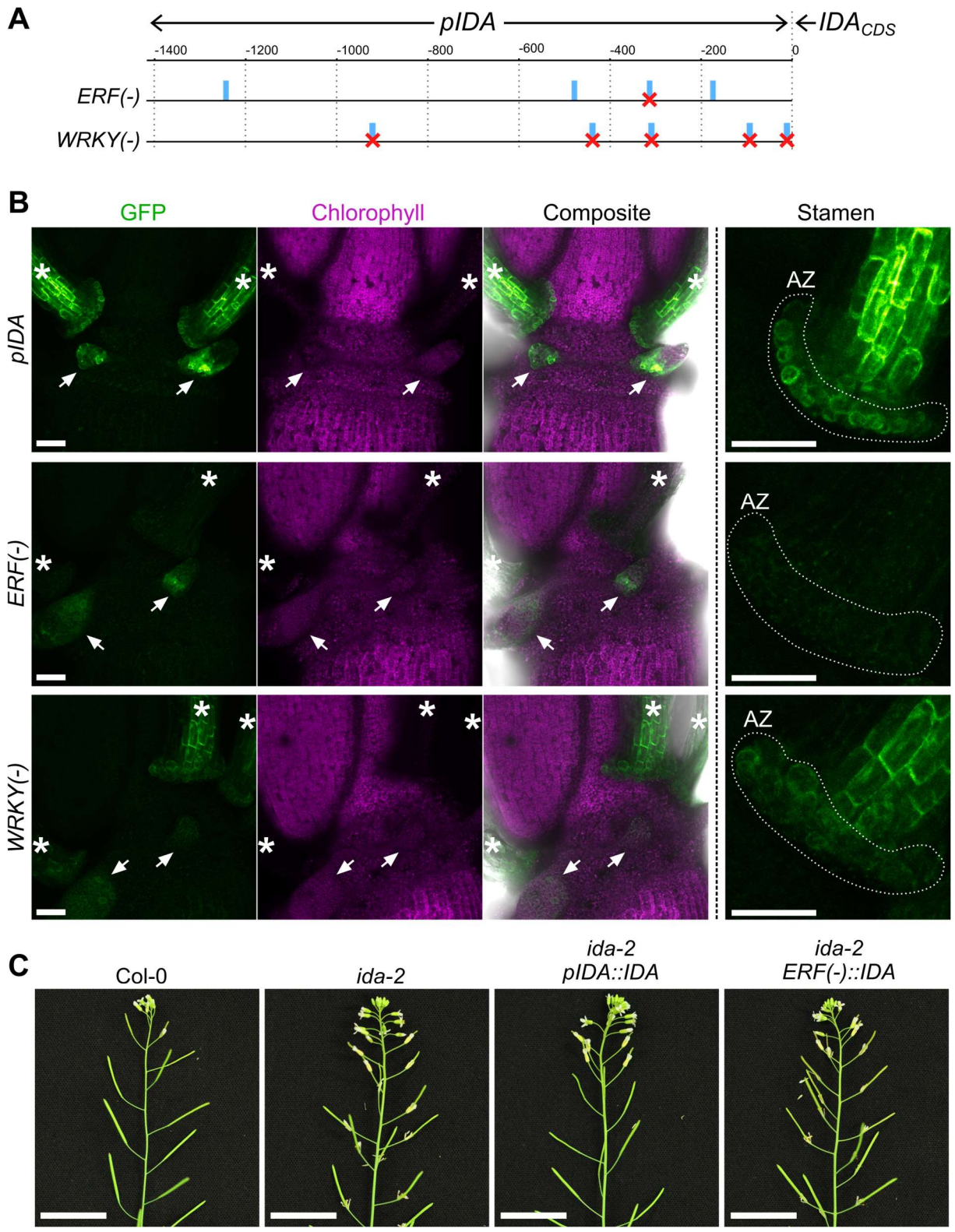

Figure 1. The *IDA* promoter activity is subject to distinct transcriptional regulation by ERF and WRKY transcription factors. **A,** Schematic diagram of the *IDA* promoter sequence and the two mutant versions: *ERF*(-) and *WRKY*(-). Numbers in the upper scale represent the distances in number of nucleotides from the translation initiation site of the *IDA* gene. Blue rectangles indicate the predicted TFBSs for ERF or WRKY TFs along the *IDA* promoter. Crosses mark the specific TFBSs that were disrupted by site-directed mutagenesis in either version of the *IDA* promoter – One ERF binding site, and five WRKY binding sites, respectively. **B,** Representative confocal micrographs of plants expressing GFP-GUS.

Each row corresponds to a promoter reporter line, indicated on the left. The GFP is shown in green, chlorophyll autofluorescence is shown in magenta. The rightmost column shows detail images of the stamen proximal region and AZ. White dotted lines highlight the AZ region from which quantitative measurements in Supplemental Figure S2B were taken. White arrows point towards nectaries. White stars highlight stamens. Scale bars at both magnifications represent 50 µm. **C,** Floral organ abscission phenotypes of *ida-2* mutants genetically complemented with the *IDA* gene under its wild-type promoter (*pIDA*) or the *ERF*(-) mutant version. Floral organs remain attached to most developing siliques in the *ERF*(-) lines, indicating lack of complementation of the *ida-2* abscission defect. Twelve out of 14 *pIDA* lines fully reverted the *ida-2* phenotype. Zero out of 20 *ERF*(-) lines fully reverted the *ida-2* phenotype. See also Supplemental Figure S4. Scale bars are 2 cm.

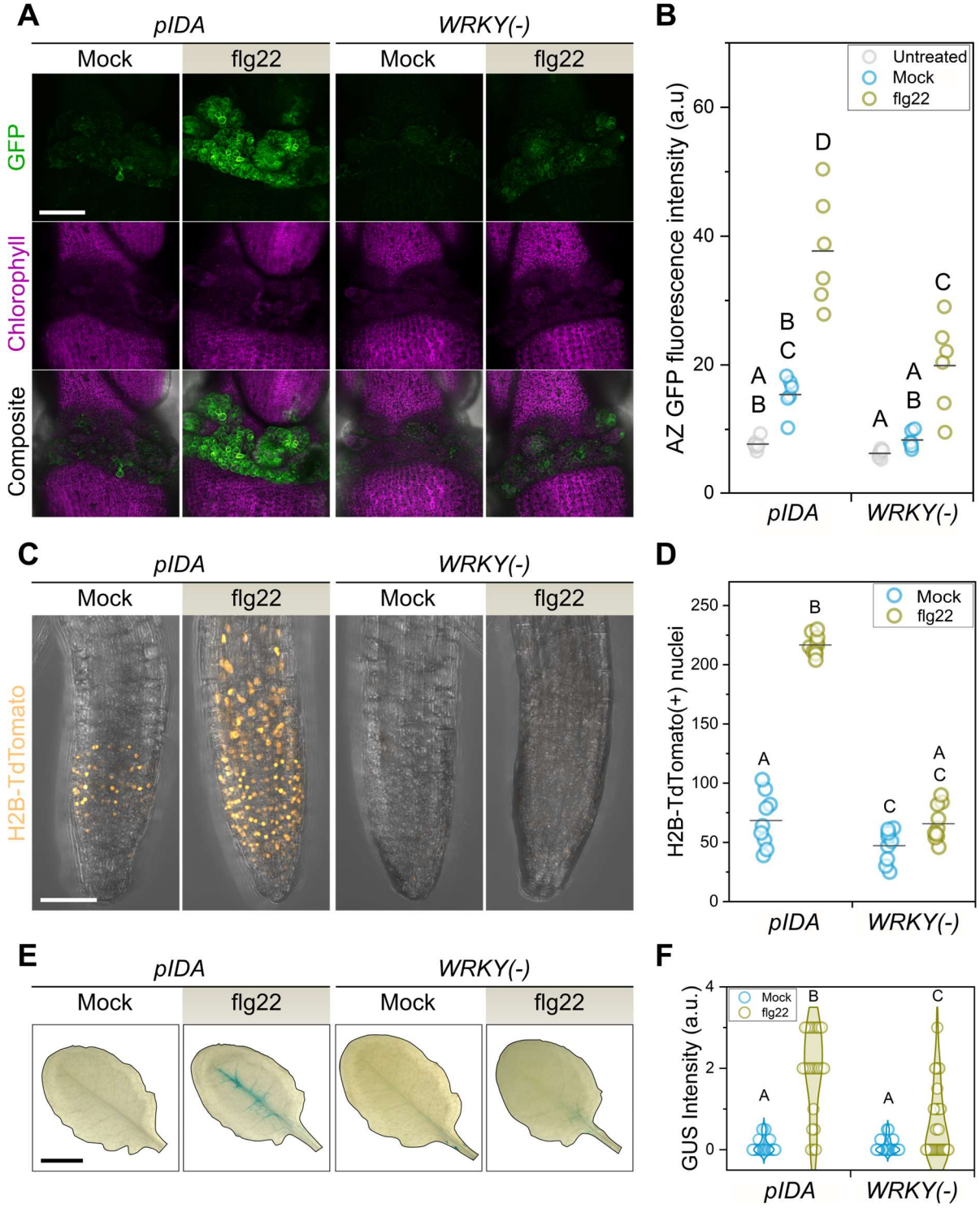

Figure 2. *IDA* responsiveness to flg22 depends on the presence of WRKY promoter binding sites. **A,** Residuum abscission zone cells induce *IDA* in response to flg22 in a WRKY TFBS-dependent manner. Reporter lines express GFP-GUS under the control of the promoters indicated on top. Scale bar represents 120 µm. Micrographs shown are maximum intensity projections of the GFP, chlorophyll autofluorescence or composite channels. Images are representative of an experiment with six plants per line, and one flower in positions six or seven per plant per treatment. The experiment was repeated twice using different transgenic lines for each reporter construct with similar results. **B,** Quantification of the GFP fluorescence intensity in the entire abscission zone area of the maximum intensity projections shown in A. Each datapoint corresponds to the average GFP intensity in the abscission zone region of one flower. **C,** The root meristematic region responds to flg22 treatment by upregulating *IDA* in a

WRKY TFBS-dependent manner. Reporter lines express H2B-TdTomato under the control of the promoters indicated on top. Images are maximum intensity projections of composite confocal micrographs. Scale bar represents 30 µm. Images are representative of an experiment with ten seedlings per line and treatment. The experiment was repeated three times with three independent lines per reporter construct and obtained similar results. **D,** Quantification of nuclei with H2B-TdTomato expression from maximum intensity projections of the root meristematic region. Each datapoint corresponds to the nuclei quantified in each individual seedling assayed. **E,** Representative images of the histochemical detection of GUS activity in mature rosette leaves in plants expressing GFP-GUS under the promoters displayed on top. Scale bar is 0.5 cm. **F,** Quantification of the beta glucuronidase (GUS) activity detected in mature leaves like the ones shown in E. Data shown here contains the dataset from three independent transgenic lines per reporter construct, totaling between 24-32 plants per construct and treatment combination. Leaf GUS staining intensity was qualitatively assessed and assigned to categories (see Materials and methods). Letters in panels B, D and F represent categories of statistically significant differences in two-way ANOVA and post hoc pairwise comparisons with Bonferroni tests ($p < 0.05$).

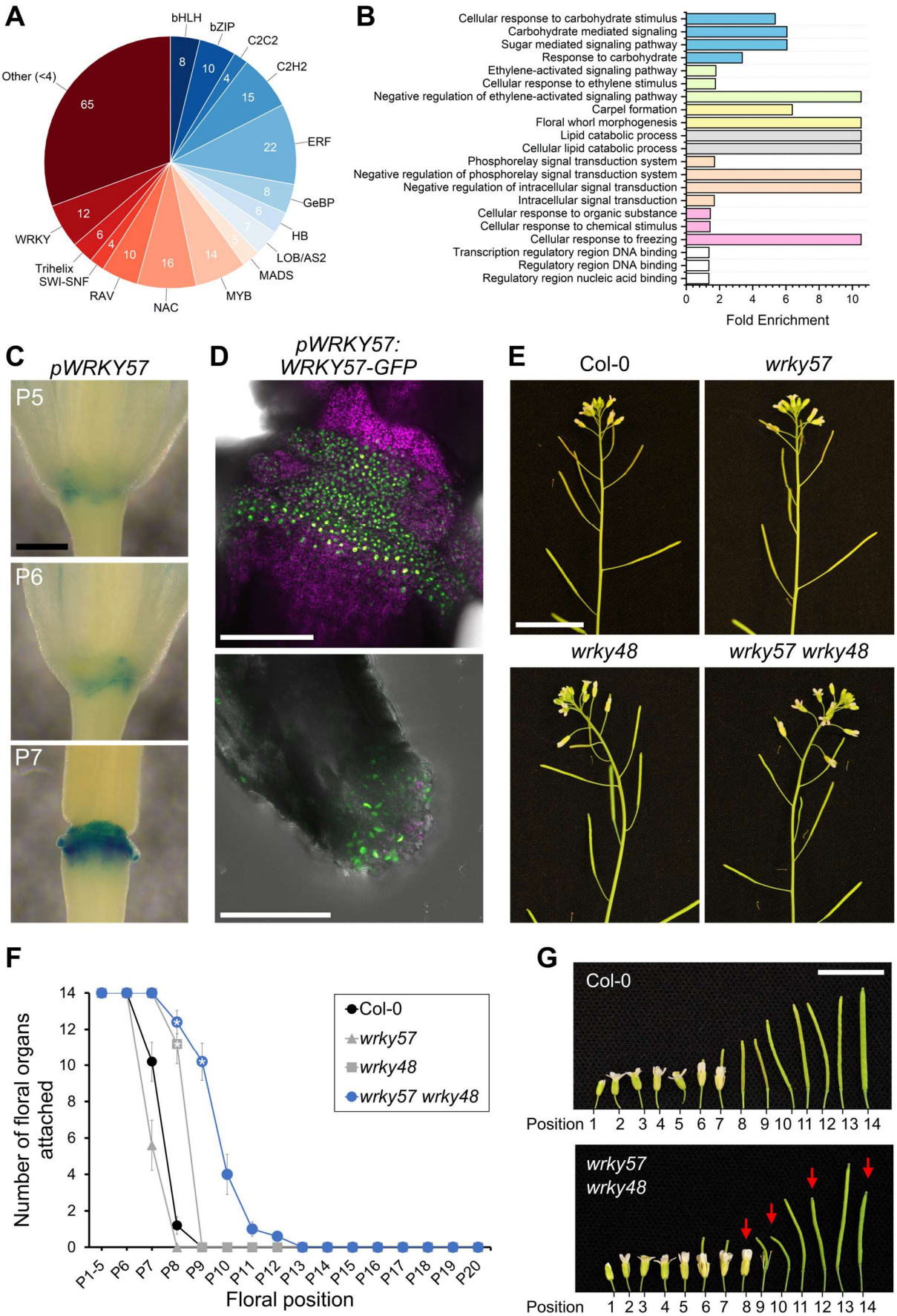

Figure 3. A screening against a collection of Arabidopsis TFs identified WRKY57 as a putative regulator of abscission. **A,** Summary of TFs identified in the Y1H screen of the *IDA* promoter. TFs are

represented by family. TF families with less than 4 members identified in the screen were grouped in the "Other" category to ease visualization. See also the Supplemental Table S3. **B,** Gene ontology term enrichment analysis of the set of 211 TFs identified in the Y1H screen. Gene ontology terms associated with the 211 TFs were compared against the reference, in this case the entire list of TFs in Arabidopsis thaliana. All terms listed here are statistically enriched at $p < 0.01$. Different colors represent related terms (blue, carbohydrates; green, ethylene; yellow, floral development; grey, lipids; orange, signaling; pink, other responses; white, DNA binding). **C,** Histochemical staining of GUS activity in plants expressing GFP-GUS under *WRKY57* promoter. Scale bar is 0.4 mm. P5, P6, P7 are floral positions five, six and seven along the main inflorescence stem. **D,** Maximum intensity projections of confocal micrographs of the AZs of plants expressing *pWRKY57:WRKY57-GFP*. On the top panel, green nuclear signals from WRKY57-GFP are seen in the residuum cells. Scale bar is 150 µm. Below, WRKY57-GFP accumulates in the secession cells of a petal. Scale bar is 50 µm. Chlorophyll autofluorescence is shown in magenta in both images. **E,** Inflorescences of T-DNA lines *wrky57*, *wrky48*, and double mutant *wrky57 wrky48*. Scale bar is 2 cm. **F,** Quantitative phenotyping of floral organ abscission in the mutant lines listed in the graph legend. Markers (circles, squares, triangles) represent the mean, and whiskers the SEM. Data corresponds to the number of floral organs fully attached to the flower at each position from five plants per genotype. One way ANOVA and post hoc Bonferroni test were used to compare the four genotypes at each position. Positions with a statistically significant difference in the mean compared to wild-type plants are highlighted with a white star ($p < 0.05$). This assay was repeated twice with similar outcomes. **G,** Irregular self-pollination in the *wrky57 wrky48* double mutant, highlighted by red arrows. Scale bar is 1 cm.

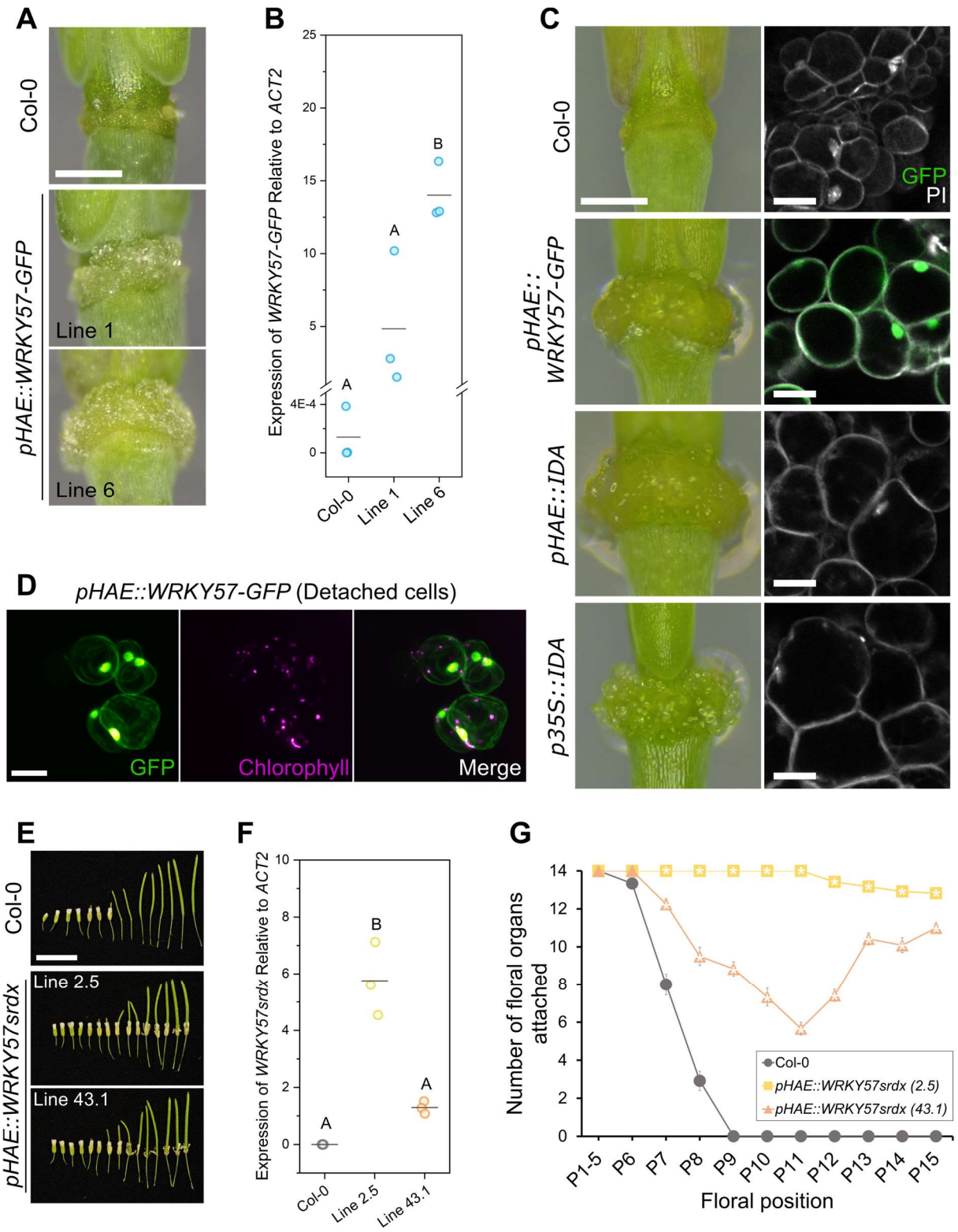

Figure 4. Modulation of floral organ abscission by local overexpression of *WRKY57*. **A,** Floral receptacles of transgenic lines in Col-0 background overexpressing WRKY57-GFP in floral position 12. Scale bar is 0.4 mm. **B,** Quantification of transgene expression levels in the transgenic lines shown in A. Datapoints are one biological replica (averaged from two technical replicas). Three biological replicas were analyzed per line. Letters denote statistically different groups at $p < 0.05$ in one way ANOVA and Bonferroni post hoc tests. *ACT2* stands for *ACTIN2*. **C,** Comparison of the AZ enlargement and cell expansion in lines locally overexpressing WRKY57, IDA, and the previously published constitutive *p35S::IDA*. See also Supplemental Figure S9. Scale bars are 0.4 mm for the panels on the

left and 20 µm in the confocal images. PI stands for propidium iodide, used to stain the cell walls (and some nuclei). GFP is shown in green and PI in grey. **D,** Example of cells that detach from the abscission zones of the *pHAE::WRKY57-GFP* lines while imaging. GFP fluorescence is shown in green, chlorophyll autofluorescence in magenta. Faint WRKY57-GFP signal can be observed in the cell periphery – most likely the cytoplasm – in samples that express the protein strongly. Scale bar represents 20 µm. **E,** Plants locally overexpressing *WRKYsrdx* in AZs strongly retain their floral organs. Scale bar represents 1 cm. **F,** Quantification of transgene expression levels in the transgenic lines shown in E. Same description as in B applies. **G,** Quantification of the floral organ abscission defect in the transgenic lines overexpressing *WRKY57srdx* in AZs. Markers (circle, square, triangle) represent the mean number of floral organs fully attached to the respective floral position. Whiskers are the SEM. White stars indicate statistically significant differences with wild-type Col-0 in one way ANOVA and post hoc Bonferroni tests at $p < 0.05$. Twelve plants per line were grown and one flower per plant and floral position was analyzed.

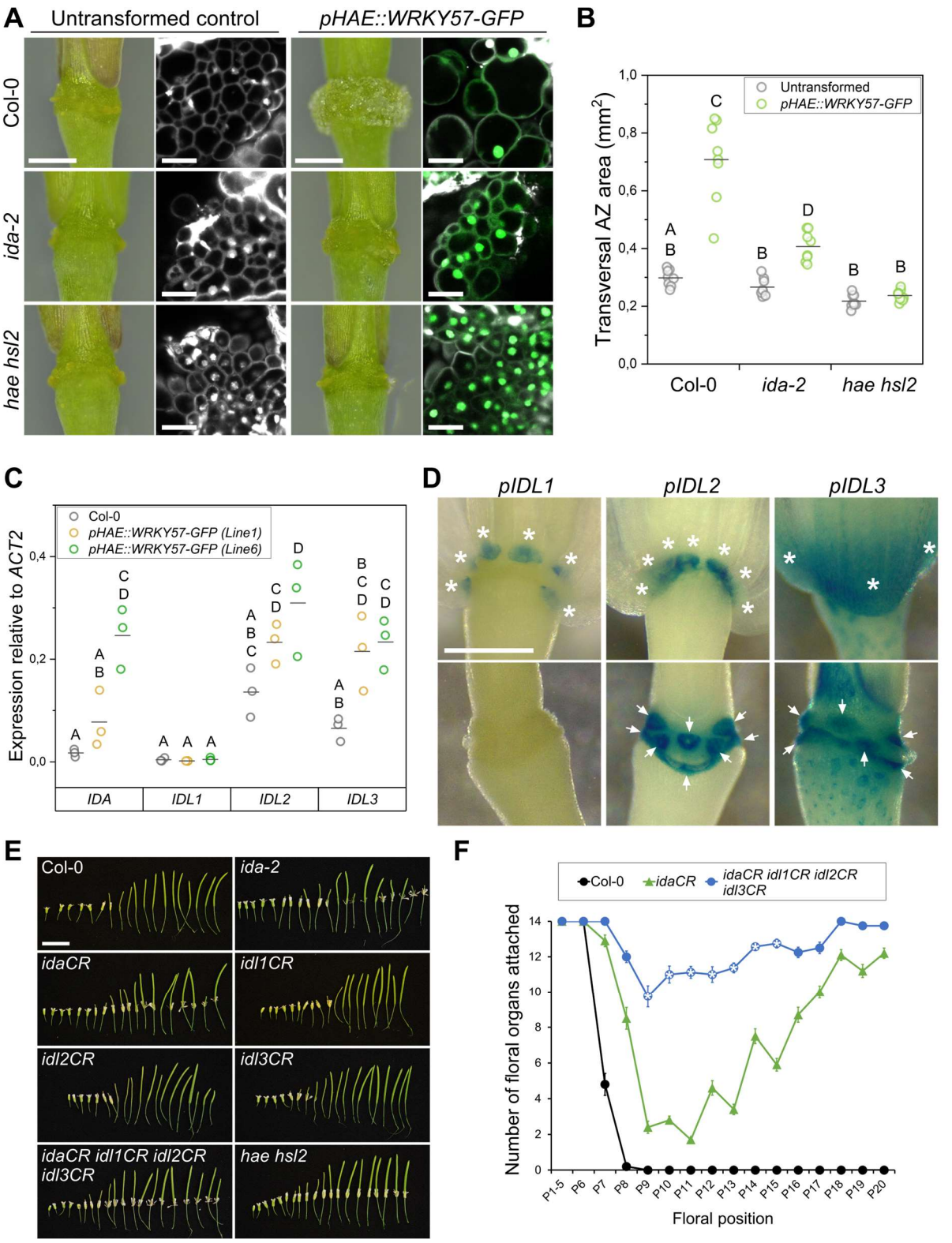

Figure 5. WRKY57 activates abscission via redundant *IDA* and *IDA-like* genes. **A,** Comparison of the AZ enlargement and cell expansion in lines locally overexpressing WRKY57-GFP in wild-type, *ida-2* and *hae hsl2* mutant backgrounds. See also Supplemental Figure S11. Scale bars are 0.4 mm for the panels on the left and 20 µm in the confocal images. GFP is shown in green and PI in grey. **B,** Quantification of the transversal AZ area in the genotypes displayed below the graph, either untransformed, or expressing the *pHAE::WRKY57-GFP* transgene. Data correspond to the measurement of the position 12 AZ area in the main inflorescence stem for each plant. Eight plants per genotype were

analyzed. Letters show statistically significant differences between groups in one-way ANOVA and Bonferroni post hoc analyses ($p < 0.05$). **C,** Estimation of gene expression of *IDA*, *IDL1*, *IDL2* and *IDL3* in the genotypes listed in the graph legend. Data correspond to the average of two technical replicates per biological replica. Three biological replicas were assayed per genotype. Letters show statistically significant differences between groups in two-way ANOVA and Bonferroni post hoc analyses ($p < 0.05$). **D,** Histochemical detection of GUS activity in plants expressing GFP-GUS under the control of the promoters listed over the panels. White stars highlight the floral organs still attached in the upper panels. White arrows point at the residuum cells with clear GUS activity in the receptacle. Scale bar represents 0.4 mm. **E,** Floral organ abscission in the genotypes listed in the panels. Scale bar represents 1 cm. **F,** Quantification of retained floral organs per floral position along the main inflorescence stem for the genotypes listed in the graph's legend. Markers (circles and triangles) represent the mean; whiskers are the SEM. White stars denote the floral positions of the quadruple *idaCR idl1CR idl2CR idl3CR* that were significantly different from *idaCR* in one way ANOVA and Bonferroni post hoc tests ($p < 0.05$). See Supplemental Figure S12 for the expanded quantification of all genotypes included in panel E.